# Modeling the dispersal of polar cod (*Boreogadus saida*) and saffron cod (*Eleginus gracilis*) early life stages in the Pacific Arctic using a biophysical transport model

Vestfals[1*a], C.D., Mueter[2], F.J., Hedstrom[3], K.S., Laurel[4], B.J., Petrik[5], C.M., Duffy-Anderson[6], J.T., and S.L. Danielson[3]

**Abstract**

Polar cod (*Boreogadus saida*) and saffron cod (*Eleginus gracilis*) are the most abundant and ecologically important forage fishes in the Pacific Arctic marine ecosystem, yet little is known about their spawning locations or the habitats occupied by their early life stages (ELS). We developed a biophysical transport model coupled to a Pan-Arctic hydrodynamic ocean circulation model to identify potential spawning locations and examine connectivity between the northern Bering, Chukchi, and Beaufort seas. We simulated the growth and transport of newly hatched polar cod and saffron cod larvae until the early juvenile stage (to 45 mm in length) using circulation model hindcasts from 2004 – 2015. Analyses identified species-specific differences in dispersal trajectories, despite similar hatch times and locations. Strong interannual variability in growth and dispersal was linked to several global-scale climate indices, suggesting that larval growth and transport may be sensitive to environmental perturbations. Results show that polar cod spawned in the northern Chukchi Sea may be an important source of larvae for the Beaufort Sea and Arctic Basin, while observed larval aggregations in the Chukchi Sea likely originated in the northern Bering and southern Chukchi seas. This study provides new information about potential spawning times and locations for polar cod and saffron cod in the Pacific Arctic and helps to identify important ELS habitat. This knowledge can help improve the management of these species and, by examining how larval connectivity changes in response to changing environmental conditions, improve our ability to anticipate how these species may respond in a rapidly changing Arctic.

Keywords: *Boreogadus saida*, *Eleginus gracilis*, early life stages, growth, dispersal, connectivity, individual-based model

[1] University of Alaska Fairbanks, College of Fisheries and Ocean Sciences, 2030 S.E. Marine Science Drive, Hatfield Marine Science Center, Newport, OR 97365, USA

[*] Corresponding author

[a]Present address: Northwest Fisheries Science Center, National Marine Fisheries Service, NOAA, 2032 S.E. OSU Drive, Newport, OR 97365, USA

E-mail: cathleen.vestfals@noaa.gov
Tel: +1 5418670524
Fax: +1 5418670505

[2] University of Alaska Fairbanks, College of Fisheries and Ocean Sciences, 17101 Point Lena Loop Rd, Juneau, AK 99801, USA

[3] University of Alaska Fairbanks, College of Fisheries and Ocean Sciences, 2150 Koyukuk Drive, Fairbanks, AK 99775, USA

[4]Alaska Fisheries Science Center, National Marine Fisheries Service, NOAA, 2030 S.E. Marine Science Drive, Hatfield Marine Science Center, Newport, OR 97365, USA

[5] Texas A&M University, Department of Oceanography, College Station, Texas 77843, USA

[6] Alaska Fisheries Science Center, National Marine Fisheries Service, NOAA, 7600 Sand Point Way N.E., Seattle, WA 98115, USA

## 1. Introduction

The Arctic is warming at an unprecedented rate. Surface air temperatures have increased at double the global rate (Screen and Simmonds, 2010) and this warming has also extended to the oceans, resulting in dramatic changes across Arctic ecosystems (Wassman et al., 2011; Huntington et al., 2020). The Pacific Arctic, in particular the Bering Strait region and the Chukchi Sea, is warming rapidly, with water temperatures increasing by 0.43 ºC per decade since 1990 (Danielson et al., 2020a). Sea-ice concentration, extent, and duration have also declined over this period, with an earlier spring ice retreat and delayed fall ice formation increasing the length of the open-water season by ~3 months (Comiso et al., 2008; Stammerjohn et al., 2012). Reduced ice cover, earlier ice melt, and greater freshwater inputs associated with warming in the Arctic are predicted to impact ecosystem dynamics via the poleward movement of boreal species and changes in marine productivity (Meredith et al., 2019). These changes will likely have a profound effect on the distribution and abundance of resident Arctic species. To better understand the consequences of these environmental changes, in this study we examine the early life stages (ELS) of polar cod (*Boreogadus saida*) and saffron cod (*Eleginus gracilis*), two of the most abundant and ecologically significant species in the Pacific Arctic marine ecosystem.

Polar cod and saffron cod play an important role in the transfer of energy to higher trophic levels, serving as key prey for piscivorous seabirds and marine mammals, as well as humans, in the northern Bering, Chukchi, and Beaufort seas (Whitehouse, 2011; Moore and Stabeno, 2015). In general, observational data for Arctic marine fishes are scarce and particularly so for their ELS, such as spawning locations, larval drift pathways, and juvenile nursery areas. Collections are mainly limited to the late spring and summer (but see Lafrance, 2009; Bouchard et al., 2016) due to the challenges and costs of sampling during winter and spring in the remote regions of the Arctic (e.g., difficulties of sampling under the ice, lack of sustained research efforts). As such, identifying major spawning locations of species that spawn under the ice during the winter, such as polar cod and saffron cod, resolving the movement and distribution of their ELS, and understanding their responses to variable climate conditions cannot be achieved through field studies alone.

Advective transport of eggs and larvae is known to play an important role in population regulation of marine fishes and several studies have linked larval transport with variability in year-class strength (Bailey, 1981; Hollowed and Bailey, 1989; Wilderbuer et al., 2002; Govoni 2005; Mueter et al., 2006; Petrik et al., 2015, 2016). Modeling approaches, such as the use of biophysical models that can track and simulate the behavior of eggs and larvae, can provide insights into the movement of ELS and information that would otherwise be unavailable through

conventional field sampling. Since eggs and larvae are relatively underdeveloped in the first few months of life, their dispersal is primarily governed by ocean circulation and can be tracked by simulating the transport of passive particles or particles with basic behaviors. Examples include temperature-dependent growth combined with size- or age-dependent vertical migrations, until the larvae grow to a size at which their movements are largely independent of the currents (Leis, 2007). The impacts of circulation on larval dispersal and recruitment has been successfully evaluated using hydrographic modeling approaches in a variety of marine systems (as reviewed in Miller, 2007), including the Gulf of Alaska and the Bering Sea (Hinckley et al., 1996; Parada et al., 2010; Duffy-Anderson et al., 2013; Vestfals et al., 2014; Petrik et al., 2015, 2016; Gibson et al., 2019).

The Chukchi Sea is a broad (> 500 km), shallow (~ 50 m deep), high-latitude shelf system that extends > 800 km northward from Bering Strait and is highly productive during the spring melt and open-water seasons (Grebmeier et al., 1988). The seasonally fluctuating Pacific-Arctic sea level gradient (Stigebrandt, 1984; Aagaard et al., 2006) drives the northward flow from the Bering Sea through the narrow (~85 km) and shallow (~50 m) Bering Strait. Water entering the Chukchi Sea is often classified into three water masses: cold, relatively saline, and nutrient-rich Anadyr Water (AW) in the west (Coachman et al., 1975; Sambrotto et al., 1984), seasonally present and relatively warm, low-salinity Alaskan Coastal Water (ACW) in the east, and a mixture of the two water masses, Bering Shelf Water (BSW) (Coachman et al., 1975), which originates primarily from 100 m isobath flow (Stabeno et al., 2018). Peak inflow through Bering Strait occurs during summer, bringing relatively fresh water, nutrients, heat, carbon, and organisms into the Chukchi and Beaufort seas (Wyllie-Echeverria et al., 1997; Weingartner et al., 2005; Woodgate et al., 2005a, b; Moore and Stabeno, 2015), while strong southward winds in winter reduce the northward flows (Woodgate et al., 2005a, b; Stabeno et al., 2018).

Inflow through Bering Strait moves across the Chukchi shelf along three main pathways: westward through Hope Valley towards Herald Canyon (Coachman et al., 1975; Weingartner et al., 2005; Woodgate and Aagaard, 2005; Pickart et al., 2010), eastward parallel to the Alaskan coastline into Barrow Canyon (Coachman et al., 1975), and through the Central Channel across the mid-shelf between Herald and Hanna Shoals (Weingartner et al., 2005) (Fig. 1). Flow across the shelf is highly variable and can be modified by local winds and other fluctuations, with particularly strong northerly winds capable of reversing the transport for periods of days to weeks (Coachman and Aagaard, 1981; Weingartner et al., 2005; Woodgate et al., 2005a, b; Danielson et al., 2014, 2017). Flow exits the Chukchi shelf through Barrow Canyon in the east (Coachman et al., 1975; Weingartner et al., 2005) or Herald Canyon in the west (Coachman et al., 1975; Pickart

et al., 2010). Water exiting through Barrow Canyon flows either westward along the Chukchi shelf break as the Chukchi Slope Current (Corlett and Pickart, 2017), or eastward into the Beaufort Sea along the shelf break and slope (Pickart, 2004). Low-salinity waters associated with river outflow and solar heating are transported northward during the summer and fall by the seasonal Alaska Coastal Current (ACC, Coachman et al., 1975). The water column cools to near freezing temperatures in the late fall and early winter and remains near the freezing point until late spring and early summer, when increasing solar radiation and the inflow of warmer water from the Bering Sea leads to rapid warming, melting of sea ice, and increased river discharge (Weingartner et al., 2005; Danielson et al., 2017, 2020a).

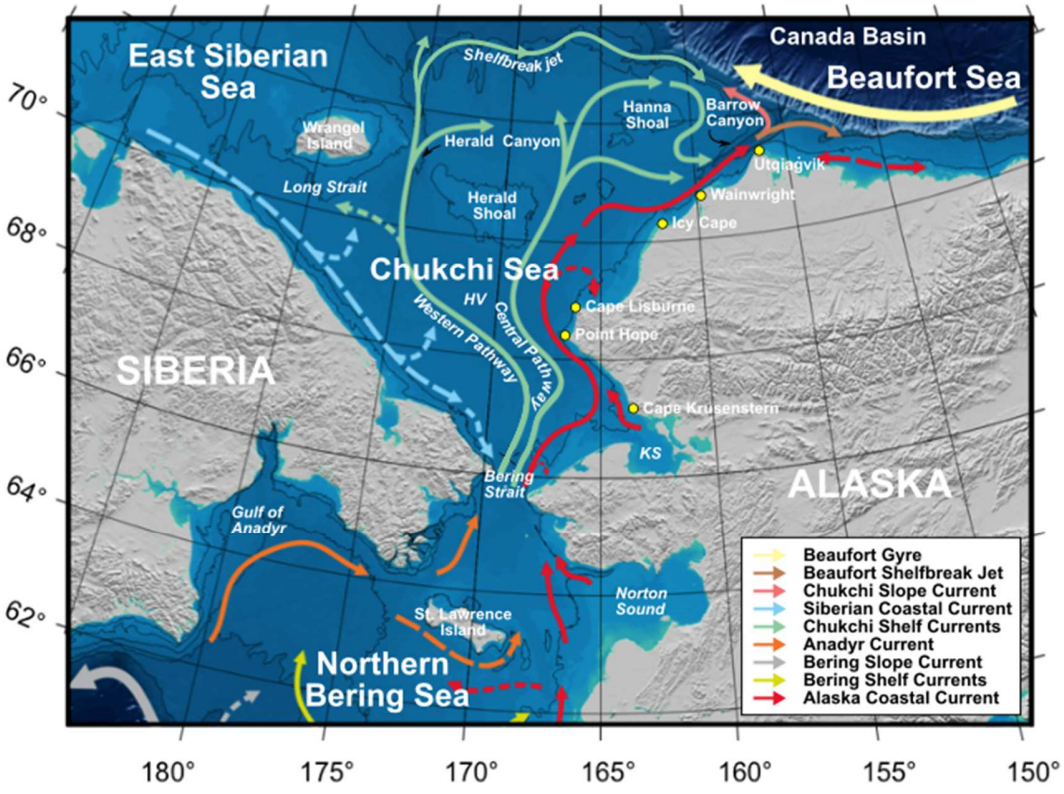


Fig. 1. Map of typical flow pathways of the northern Bering Sea, Chukchi Sea, and western Beaufort Sea based on Danielson et al. (2020a) with water bodies and place names. Persistent currents are shown with solid arrows; intermittent or poorly known flows are shown with dashed arrows. KS denotes Kotzebue Sound and HV denotes Hope Valley. Depth isopleths are contoured with thin black lines at 25, 70, 100, and 200 m.

Building on previous modeling efforts for walleye pollock (*Gadus chalcogrammus*) in the eastern Bering Sea (Petrik et al., 2015, 2016) and using an ocean circulation model for the Arctic region, we developed biophysical transport models parameterized for larval and early juvenile stages of polar cod and saffron cod. These models were used to simulate the growth and dispersal of their ELS in the northern Bering, Chukchi, and Beaufort seas to identify possible spawning locations, which are currently largely unknown, as well as examine connectivity between these regions. Several behavior scenarios were tested and modeled distributions were compared to known summer distributions of larvae and early juveniles from acoustic-trawl surveys conducted in 2012 and 2013 in the northern Bering and Chukchi seas. Selected behavior scenarios were then used to model their growth and dispersal from 2004 – 2015 to assess interannual variability relative to oceanographic and atmospheric conditions. In addition to providing important information about potential spawning areas and nursery habitats of polar cod and saffron cod, this research helps establish whether observed aggregations of larvae and early juveniles are likely to be retained in the Chukchi Sea, contributing primarily to local populations, or if they are likely to be transported from the northern Chukchi Sea into the Beaufort Sea, thereby serving as a source population for gadids in the Beaufort Sea. This research also provides valuable information about the growth and dispersal of Arctic gadids under variable climate conditions, which is important for understanding how these species respond to environmental perturbations and how their connectivity between the Chukchi and Beaufort seas may be impacted.

## 2. Methods

### 2.1. Circulation model

To realistically simulate the three-dimensional (3-D) circulation field and force the Lagrangian particle-tracking model, we used an implementation of the state-of-the-art, free-surface Regional Ocean Modeling System (ROMS; Shchepetkin and McWilliams, 2005) set up in a Pan-Arctic (PAROMS) configuration (Curchitser et al., 2013, Danielson et al., 2016, 2020b; Lovvorn et al., 2020). The domain of this coupled ocean/sea-ice numerical model spans the Arctic from the Bering Sea in the North Pacific to the North Atlantic. The horizontal resolution varies from ~ 5 km south of the Aleutian Islands to ~9 km in the North Atlantic and is approximately 5.5 – 6.0 km in the Chukchi Sea. The 50-layer vertical coordinate system is based on terrain-following sigma-layers with finer resolution within the surface and bottom boundary layers. PAROMS is forced by NASA's Modern-Era Retrospective-Analysis for Research and Applications atmospheric reanalysis (Rienecker et al., 2011), with boundary conditions coming

from the Simple Ocean Data Assimilation (SODA, Carton and Giese, 2008) for 2008 and prior, and from the Hybrid Coordinate Ocean Model (HYCOM; Chassignet et al., 2009) for more recent years. Tidal forcing is provided by the Oregon State TOPEX/Poseidon Global Inverse Solution (Egbert and Erofeeva, 2002) and the sea ice field is based on the single-category Budgell ice model (Budgell, 2005). For surface fresh water flux, the model uses the method of Dai et al. (2009) south of the Yukon River and that of Whitefield et al. (2015) for the Arctic. A careful model-to-observation comparison of hindcast velocity, temperature, and salinity in the Chukchi and Beaufort seas found that the model exhibited appreciable skill in reproducing the mean velocity directions and magnitudes and the velocity variances at time scales from tidal to annual (Curchitser et al., 2013). The model also captured synoptic and seasonal temperature, salinity, and stratification variations. Offshore ice thicknesses in mid-winter were found by Curchitser et al. (2013) to generally be within 1 m of those estimated from the IceSat satellite missions (Kwok et al., 2009). Without restoring sea ice concentrations to observational data or data assimilation, the model reproduced approximately 50% of both the observed monthly and annual ice concentration anomalies (Curchitser et al., 2013). Additional model-data comparisons that demonstrate model fidelity in reproducing wind-driven SSH anomalies are provided in Danielson et al. (2020b).

Output from the PAROMS 2004 – 2015 hindcast was saved as daily averages to force the offline particle-tracking model, as described below. Specifically, the particle-tracking model used PAROMS-generated velocities, temperature, and salinity.

**2.2 Particle tracking**

To simulate advective transport and growth of larvae, we developed individual-based models (IBMs) for polar cod and saffron cod using the particle tracking tool TRACMASS, which calculates Lagrangian trajectories from Eulerian velocity fields (Döös, 1995). The TRACMASS model is run offline using stored daily output from PAROMS integrations, thus it is less computationally expensive and allows for more calculations of trajectories in comparison to those made online within the circulation model. TRACMASS runs on the 3-D PAROMS grid and solves the trajectory path through each grid cell with an analytical solution of a differential equation, which depends on the horizontal and vertical velocities at the grid cell walls (Döös, 1995). TRACMASS has been used in atmospheric and oceanic studies (Drijfhout et al., 2003; Döös and Engqvist, 2007), as well as for modeling the dispersal of fish and invertebrate larvae (Jacobi and Jonsson, 2011; Berglund et al., 2012; Petrik et al., 2015, 2016).

The particle-tracking time step used in TRACMASS was 1 hour and sub-grid scale turbulence was incorporated by adding a random horizontal turbulent velocity to the horizontal

velocity from PAROMS to each trajectory and each horizontal grid wall at every time step (Döös and Engqvist, 2007). A horizontal diffusion value of 4 $m^2 s^{-1}$ was used, based on the relationship between diffusion and model resolution defined in Okubo (1971). Model output of position (latitude and longitude), temperature, salinity, and larval length (see Section 2.3 below) was saved at daily intervals. In addition to particle trajectories, TRACMASS calculated surface light as a function of latitude, longitude, date, and time of day for behavior scenarios that included diel vertical migrations (DVM). While TRACMASS had impermeable boundary conditions at the coast, the incorporation of diffusion into the model allowed for beaching of simulated particles. Trajectories of particles that beached were no longer tracked in the model. Particles rebounded from ice.

We based the number of particles released for each dispersal simulation on the method described in Petrik et al. (2015). In that study, the number of particles released at each time and location (number of simulation repetitions) was determined by calculating the fraction of particles at four random locations downstream of the initial start locations. The minimum number of particles for which those fractions did not change appreciably was determined, with 10 particles per 10 m depth increment per spawning location deemed appropriate for producing stable results (Petrik et al., 2015). For our study, we doubled the number of particles, given that the Chukchi Sea is shallower than the Bering Sea, releasing 10 particles per 5 m depth increment at each PAROMS grid point within each release location (Table 1). Due to the lack of information available about the vertical distributions of post-hatch polar cod and saffron cod larvae in the water column at the time of this study, simulated larvae were released every 5 m from the surface to the bottom. Since saffron cod spawn in close proximity to the bottom (Chen et al., 2008) and their eggs are demersal and adhesive (Berg, 1949; Wolotira, 1985), spawning and hatching locations were assumed to be identical, with dispersal simulations reflecting dispersal from their spawning grounds. For the initial simulations, the minimum and maximum number of particles released were 15,480 and 289,220, respectively, for a total of 623,510 particles released across all locations on each simulation date (Table 1).

Table 1. Hypothesized spawning and/or hatching areas of polar cod (*Boreogadus saida*) and saffron cod (*Eleginus gracilis*), region, number of PAROMS grid points, and number of particles released for each dispersal simulation.

| Hatch area | Region | # of grid points | # of particles |
|---|---|---|---|
| Gulf of Anadyr | Bering Sea | 3,347 | 289,220 |
| St. Lawrence Island | Bering Sea | 235 | 15,480 |
| Norton Sound | Bering Sea | 735 | 19,370 |
| Bering Strait | Bering Sea | 663 | 48,530 |
| Chukotka Peninsula | Chukchi Sea | 888 | 57,550 |
| Kotzebue Sound | Chukchi Sea | 534 | 20,790 |
| Cape Lisburne | Chukchi Sea | 700 | 45,690 |
| Hanna Shoal | Chukchi Sea | 759 | 68,750 |
| Barrow Canyon | Chukchi Sea | 616 | 58,130 |
| Total | | 8,477 | 623,510 |

241
242
243 **2.3. Biological model**
244 **2.3.1. Growth**
245 Temperature-dependent growth rates have recently been estimated for larval polar cod
246 and saffron cod in the laboratory (Koenker et al., 2018; Laurel et al., 2018; B. Laurel, National
247 Oceanic and Atmospheric Administration (NOAA), unpublished results). These data provide the
248 information necessary for parameterizing models such as the one presented in this study and
249 provide temperature-dependent growth and developmental rates from the newly hatched larvae to
250 ~25 mm for polar cod and 10 mm for saffron cod. All growth models were based on food
251 'unlimited' scenarios.
252
253 **2.3.1.1. Polar cod**
254 *Egg stage*: Despite the availability of a temperature-dependent equation for egg development,
255 simulations were initialized at the time of hatching due to uncertainties about where in the water
256 column polar cod eggs occur (e.g., whether they are frozen into the sea ice (Yudanov, 1976) or
257 float at the ice-water interface) and uncertainties about the ability of the PAROMS model to
258 accurately capture small-scale under-ice flow dynamics. Currently, sea ice in PAROMS is
259 modeled as a flat-bottomed surface; however, sea ice is a complex surface that can vary
260 dramatically across even short distances, with ice keels in the Chukchi Sea regularly exceeding
261 20 m in depth (Hauri et al., 2018). Thus, in an attempt to minimize uncertainties in drift
262 trajectories and ensure more realistic growth and transport of ELS, simulations were restricted to
263 the post-hatch period.
264
265 *Yolksac larvae*: Yolksac larvae were initialized at a random hatch length selected from a normal

distribution with a mean standard length (SL) of 5.70 mm and standard deviation (SD) of 0.48 mm. These values were obtained from temperature incubation experiments of polar cod eggs from Beaufort Sea broodstock (Laurel et al., 2018).

*Preflexion larvae*: Growth from hatch to 10 mm (Fig. 2 a) was modeled as a function of temperature (T) as:

$$\text{Growth (mm day}^{-1}) = 0.0735 + 0.0149*T - 0.0013*T^2,$$

with coefficients determined from a polynomial regression (Koenker et al., 2018).

*Post-flexion larvae*: Due to the lack of temperature-dependent growth data available for larger sizes, growth from 10 – 25 mm (Fig. 2 a) was modeled using a temperature-dependent growth equation derived for polar cod larvae 10 – 15 mm in length (Koenker et al., 2018):

$$\text{Growth (mm day}^{-1}) = 0.0369 + 0.0583*T - 0.0044*T^2$$

*Late-larvae/early juvenile*s: Growth from 25 – 45 mm (Fig. 2 a) was modeled using a temperature-dependent growth equation for early juveniles between 45 – 70 mm in length (> 10 weeks old, Laurel et al., 2017), as temperature-dependent growth data were not available for these sizes:

$$\text{Growth (mm day}^{-1}) = 0.1377 + 0.0311*T + 0.0041*T^2 - 0.0004*T^3$$

Larval length was only updated for nonnegative growth rates, thereby preventing larvae from shrinking at lower temperatures.

**2.3.1.2. Saffron cod**

*Egg stage*: Similar to polar cod, the egg stage of saffron cod was not included in our simulations, despite the availability of information about temperature-dependent egg development. Simulations were initialized at the time of hatching due to uncertainties about the ability of the PAROMS model to accurately capture small-scale under-ice flow dynamics (see Section 2.3.2.1 above). Thus, in an attempt to minimize uncertainties in drift trajectories and ensure more realistic growth and transport of ELS, simulations were restricted to the post-hatch period.

*Yolksac larvae*: Yolksac larvae were initialized at a random hatch length selected from a normal distribution with a mean SL of 5.44 mm and SD of 0.30 mm based on values obtained from temperature incubation experiments of saffron cod eggs from Gulf of Alaska broodstock (B. Laurel, NOAA, unpublished results). Size at hatch was not related to incubation temperature.

*Preflexion larvae*: Growth from hatch to 10 mm (Fig. 2 b) was modeled as:

$$\text{Growth (mm day}^{-1}) = 0.0016 + 0.0088*T$$

*Flexion larvae – early juveniles*: At present, temperature-dependent growth models for larval saffron cod > 10 mm in length are not available. Growth of saffron cod at these small sizes is linear and resembles that of walleye pollock (B. Laurel, NOAA, unpublished results). Assuming that growth of larger saffron cod remains similar to that of larger walleye pollock, we used the walleye pollock growth model described in Porter and Bailey (2007) and Petrik et al. (2015) to model saffron cod growth from 10 mm to 45 mm (Fig. 2 b).

$$\text{Growth (mm day}^{-1}) = 0.0902 * \log(T) - 0.0147$$

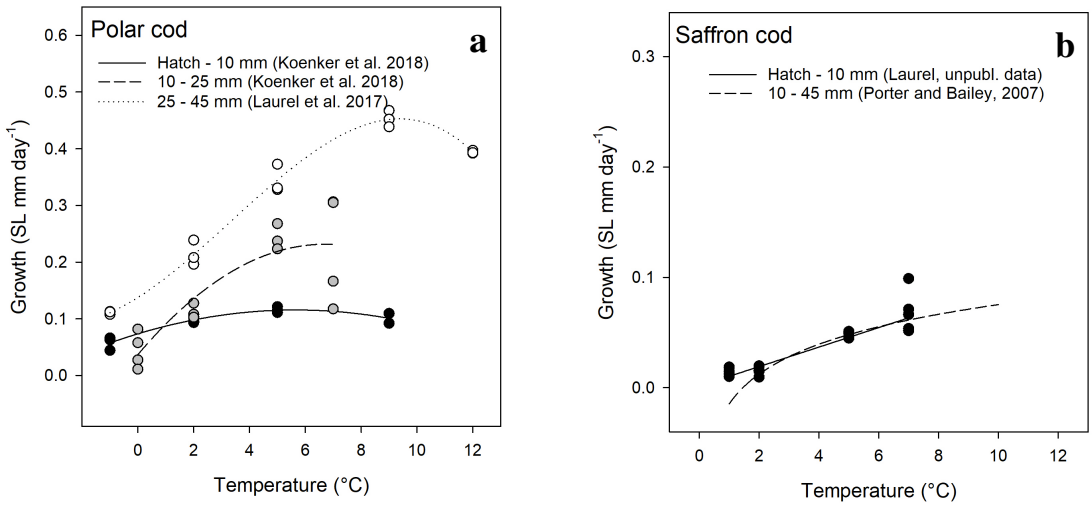


Fig. 2. Temperature-dependent growth rates (in mm day$^{-1}$) used to model growth of (a) polar cod (*Boreogadus saida*) and (b) saffron cod (*Eleginus gracilis*) early life stages in the individual-based models (IBMs). Growth rates for polar cod yolksac (hatch – 10 m) and feeding (10 – 25 mm) larvae in the model were based on those derived in Koenker et al. (2018), while early

juvenile growth (25 – 45 mm) was based on Laurel et al. (2017). The growth rate for saffron cod yolksac larvae (hatch to 10 mm) was based on unpublished data (B. Laurel, NOAA). For growth of saffron cod preflexion larvae to early juveniles (10 – 45 mm), the walleye pollock (*Gadus chalcogrammus*) growth model described in Porter and Bailey (2007) was used, as a saffron cod-specific growth model for larger sizes is not available and walleye pollock exhibit similar growth (B. Laurel, NOAA, personal communication).

### 2.3.2. Vertical behavior

Vertical behaviors selected for polar cod were based on values obtained from the literature (Borkin et al., 1986; Bouchard et al., 2016) and from laboratory observations (B. Laurel, NOAA, unpublished results). Similar behaviors were used for the saffron cod simulations, as no information on the vertical distribution of saffron cod larvae is currently available. Five different vertical behavior scenarios were developed and tested: (1) passive (neutrally buoyant) individuals at all stages; (2) surface-oriented individuals such that all stages move to the middle of the 10-m surface layer at 5 m; (3) passive yolksac larvae where older stages move progressively deeper in the water column: preflexion/flexion larvae (5 – 10 m), transformation (10 – 15 m) and early juveniles (20 m); (4) surface-oriented yolksac larvae and older individuals that move progressively deeper in the water column; and (5) surface-oriented yolksac larvae and transformation and early juvenile stages that make diel vertical migrations (DVMs) to the middle of the surface layer (5 m) at night (Table 2). For DVM, day was defined as times when surface light was greater than zero.

Table 2. Model parameters for different behaviors tested for polar cod (*Boreogadus saida*) and saffron cod (*Eleginus gracilis*). Passive = passive (neutrally buoyant) individuals of all stages; Surface = surface-oriented individuals of all stages; Passive & ontogeny = passive yolksac and preflexion larvae with late larvae and early juveniles moving deeper with ontogeny; Surface & ontogeny = surface-oriented yolksac and preflexion larvae with late larvae and juveniles moving deeper with ontogeny; DVM = surface-oriented yolksac and preflexion larvae with late larvae and early juveniles making diel vertical migrations (DVMs) between specified depths during the day, and 5 m during the night. $w_{max}$ = maximum vertical swimming speed, nb =neutrally buoyant, trans = transformation, early juv. = early juvenile.

| Polar cod | | | | | | |
|---|---|---|---|---|---|---|
| **Behavior** | **Length (mm)** | **Stage** | **$w_{max}$ (m s$^{-1}$)** | **Daytime depth (m)** | **Nighttime depth (m)** | **Temperature-dependent growth** |
| **Passive** | hatch - 10 | yolksac, preflexion | 0.002 - 0.003 | nb | nb | Koenker et al. (2018) |
| | 10 - 25 | post-flexion | 0.003 - 0.008 | nb | nb | Koenker et al. (2018) |
| | 25 - 45 | trans - early juv. | 0.008 - 0.014 | nb | nb | Laurel et al. (2017) |
| **Surface** | hatch - 10 | yolksac, preflexion | 0.002 - 0.003 | 5 | 5 | Koenker et al. (2018) |
| | 10 - 25 | post-flexion | 0.003 - 0.008 | 5 | 5 | Koenker et al. (2018) |
| | 25 - 45 | trans - early juv. | 0.008 - 0.014 | 5 | 5 | Laurel et al. (2017) |
| **Passive & ontogeny** | hatch - 10 | yolksac, preflexion | 0.002 - 0.003 | nb | nb | Koenker et al. (2018) |
| | 10 - 25 | postflexion | 0.003 - 0.008 | 8 | 8 | Koenker et al. (2018) |
| | 25 - 30 | transformation | 0.008 - 0.009 | 12 | 12 | Laurel et al. (2017) |
| | 30 - 45 | early juvenile | 0.009 - 0.014 | 20 | 20 | Laurel et al. (2017) |
| **Surface & ontogeny** | hatch - 10 | yolksac, preflexion | 0.002 - 0.003 | 5 | 5 | Koenker et al. (2018) |
| | 10 - 25 | postflexion | 0.003 - 0.008 | 8 | 8 | Koenker et al. (2018) |
| | 25 - 30 | transformation | 0.008 - 0.009 | 12 | 12 | Laurel et al. (2017) |
| | 30 - 45 | early juvenile | 0.009 - 0.014 | 20 | 20 | Laurel et al. (2017) |
| **DVM** | hatch - 10 | yolksac, preflexion | 0.002 - 0.003 | 5 | 5 | Koenker et al. (2018) |
| | 10 - 25 | postflexion | 0.003 - 0.008 | 8 | 5 | Koenker et al. (2018) |
| | 25 - 30 | transformation | 0.008 - 0.009 | 12 | 5 | Laurel et al. (2017) |
| | 30 - 45 | early juvenile | 0.009 - 0.014 | 20 | 5 | Laurel et al. (2017) |

| Saffron cod | | | | | | |
|---|---|---|---|---|---|---|
| **Behavior** | **Length (mm)** | **Stage** | **$w_{max}$ (m s$^{-1}$)** | **Daytime depth (m)** | **Nighttime depth (m)** | **Growth** |
| **Passive** | hatch - 10 | yolksac, preflexion | 0.002 - 0.003 | nb | nb | Laurel (unpublished data) |
| | 10 - 45 | postflexion - early juv | 0.003 - 0.014 | nb | nb | Porter and Bailey (2007) |
| **Surface** | hatch - 10 | preflexion | 0.002 - 0.003 | 5 | 5 | Laurel (unpublished data) |
| | 10 - 45 | postflexion - early juv. | 0.003 - 0.014 | 5 | 5 | Porter and Bailey (2007) |
| **Passive & ontogeny** | hatch - 10 | yolksac, preflexion | 0.002 - 0.003 | nb | nb | Laurel (unpublished data) |
| | 10 - 24 | flexion - postflexion | 0.003 - 0.007 | 8 | 8 | Porter and Bailey (2007) |
| | 24 - 27 | transformation | 0.007 - 0.008 | 12 | 12 | Porter and Bailey (2007) |
| | 27 - 45 | early juvenile | 0.008 - 0.014 | 20 | 20 | Porter and Bailey (2007) |
| **Surface & ontogeny** | hatch - 10 | yolksac, preflexion | 0.002 - 0.003 | 5 | 5 | Laurel (unpublished data) |
| | 10 - 24 | flexion-postflexion | 0.003 - 0.007 | 8 | 8 | Porter and Bailey (2007) |
| | 24 - 27 | transformation | 0.007 - 0.008 | 12 | 12 | Porter and Bailey (2007) |
| | 27 - 45 | early juvenile | 0.008 - 0.014 | 20 | 20 | Porter and Bailey (2007) |
| **DVM** | hatch - 10 | yolksac, preflexion | 0.002 - 0.003 | 5 | 5 | Laurel (unpublished data) |
| | 10 - 24 | flexion - postflexion | 0.003 - 0.007 | 8 | 5 | Porter and Bailey (2007) |
| | 24 - 27 | transformation | 0.007 - 0.008 | 12 | 5 | Porter and Bailey (2007) |
| | 27 - 45 | early juvenile | 0.008 - 0.014 | 20 | 5 | Porter and Bailey (2007) |

Vertical swimming speed ($w$) was parameterized for both polar cod and saffron cod as:

$$w = w_{max} * (-\tanh(0.2 * (z - z_{pref})))$$

where $z$ is depth (m), $z_{pref}$ (m) is the preferred depth (middle of depth range or day-time/night-time preferred depths), and the maximum vertical swimming speed, $w_{max}$ (m $s^{-1}$), is

$$w_{max} = 0.3 * L_{larva} * 10^{-3}$$

where $L_{larva}$ is larval length (mm).

The swimming speed of fish larvae is often overestimated in IBMs (Peck et al., 2006); therefore, we chose a maximum speed of 0.3 body-lengths $s^{-1}$ as a conservative estimate for sustained swimming. This value aligns well with that used to model polar cod growth in the Greenland Sea and Baffin Bay (Thanassekos and Fortier, 2012) and is comparable to swimming speeds used in studies of Atlantic cod (*Gadus morhua*) larvae (Sundby and Fossum, 1990; Björnsson, 1993; Vikebø et al., 2007).

## 2.4. Simulations

### 2.4.1. Release locations and hatch dates

Larvae were released from several hypothesized hatching locations based on information from a review of the literature, anecdotal evidence, and known areas of retention in the region (Craig et al., 1982; Wolotira, 1985; Sunnanå and Christiansen, 1997; A. Whiting, Native Village of Kotzebue, personal communication). In total, nine locations were selected from which to initialize the dispersal simulations: the Gulf of Anadyr, St. Lawrence Island, Norton Sound, Bering Strait, Chukotka Peninsula, Kotzebue Sound, Cape Lisburne, Hanna Shoal, and Barrow Canyon (Table 1). Ellipses were created around the hypothesized hatching locations (Fig. 3) using ArcGIS 10.4 (ESRI, 2017) and simulations were initialized from all PAROMS grid points falling within each ellipse. Points on land were excluded.

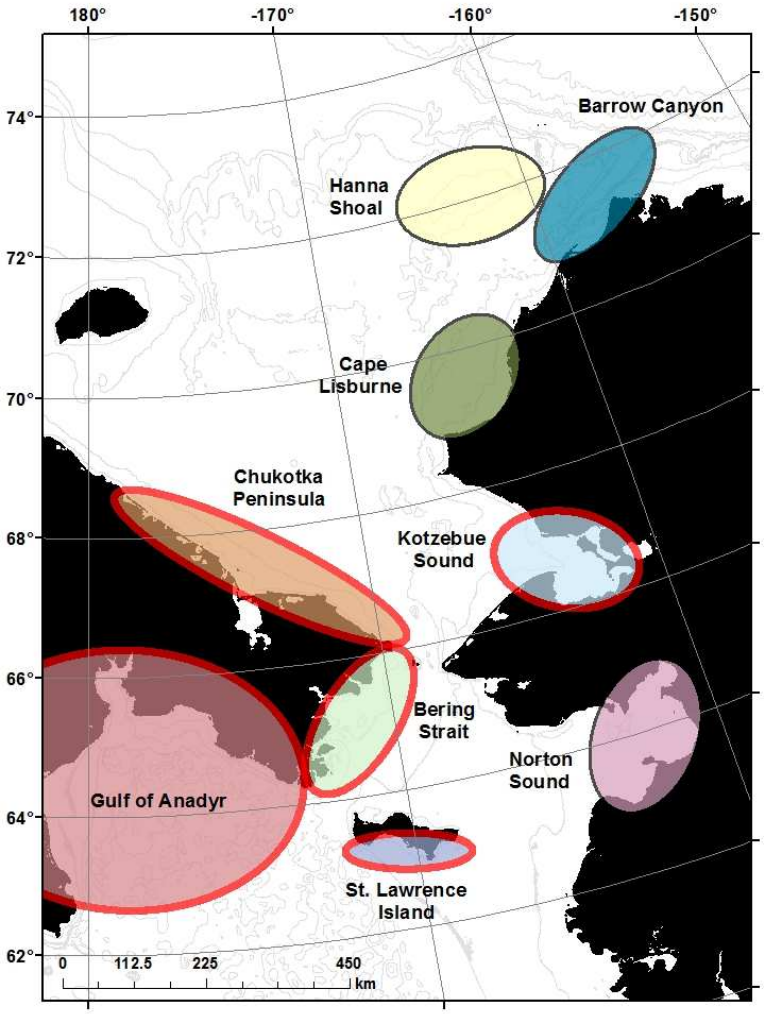


386

387 Fig. 3. Map of polar cod (*Boreogadus saida*) and saffron cod (*Eleginus gracilis*) hypothesized
388 spawning and/or hatching locations used to develop the biophysical transport models. All 9
389 locations were used for the initial dispersal simulations to select plausible release locations. Areas
390 highlighted in red were used to test 5 different behavior scenarios against 2012 and 2013 Arctic
391 Ecosystem Integrated Survey acoustic-trawl survey observations. Simulations for 2004 through
392 2015 were initiated from the Bering Strait and Chukotka Peninsula locations for polar cod, and
393 the Bering Strait and Kotzebue Sound locations for saffron cod.

394

395 In other Arctic seas, peak hatching of polar cod eggs occurs in May and June (Yudanov,
396 1976; Bouchard and Fortier, 2008), though it can occur as early as December and January in
397 regions warmed by large inputs of fresh water and as late as August in colder regions (Bouchard

and Fortier, 2011). In the Chukchi Sea, hatching can occur as late as July (Wyllie-Echeverria et al., 1997). Initial particle releases were based on a hatch date calculated from the midpoint of when polar cod were encountered in the Chukchi Sea portion of the Arctic Eis survey in 2013. The approximate hatch date was estimated by back-calculating from the average length of age-0 polar cod observed in the survey (~35.2 mm) using the regression of length on hatch date in Bouchard and Fortier (2011). This method resulted in an estimated hatch date of Julian day 72.5 (± 31.5 days SD), with most larvae hatching around early to mid-March (Marsh et al., 2019). Initially, simulated larvae hatched every two weeks from 15 February through 15 May, for a total of 7 hatching events in each year. Simulations were conducted separately for each release location and each hatch date. Results from the initial simulations suggested that larvae did not have sufficient time to achieve the lengths observed in the field, therefore, hatch dates were expanded to include the 1$^{st}$ and 15$^{th}$ day of each month from 1 January through 15 May for a total of 10 polar cod hatching events in each year. This range of hatch dates was also supported by otolith-derived ages of polar cod collected during the Arctic Eis survey (Z. Chapman, University of Alaska Fairbanks, personal communication) and allowed simulated fish lengths to better match field observations. The same range of hatch dates was used for the saffron cod simulations.

**2.4.2. Particle tracking**

Particle trajectories were tracked forward in time. While tracking particles backward in time can be used to identify potential source locations (e.g., Christensen et al., 2007; Calò et al., 2018), processes such as physical diffusion are not reversible in time (Batchelder, 2006). Backtracking can be complicated by ontogenetic development and the active behavior of larvae due to the stochastic and nonlinear nature of these processes (Christensen et al., 2007). Backtracking may be more suitable for short-duration simulations, but is less effective in shallow, nearshore regions with strong flow–bathymetry interactions (Batchelder, 2006, Bauer et al., 2013). Although inefficient and computationally expensive (Batchelder, 2006; Christensen et al., 2007), tracking particles forward in time can be used to evaluate retention in suitable areas, transport to nursery grounds, or loss to unfavorable habitats (Christensen et al., 2007). Given the shallow Chukchi shelf (~ 50 m deep), the long drift duration (see Section 2.4.3. below), and the incorporation of diffusion and behavior in our simulations, backtracking was not implemented. The feasibility of tracking fish larvae backwards from observed distributions for several months was uncertain and may have resulted in overly broad distributions. Furthermore, backtracking in TRACMASS did not allow for active behavior of the particles at the time of publication.

### 2.4.3. Duration of simulated drift

Growth and dispersal of larvae were simulated until 1 September, the midpoint of the Arctic Eis survey, so that the simulated distribution and size composition during summer could be compared to the observed distributions and size compositions in the 2012 and 2013 Arctic Eis acoustic-trawl surveys. Polar cod and saffron cod transition from pelagic juveniles to more demersally-oriented juveniles at approximately 35 – 45 mm (ICES CM, 1988) and between 39 – 60 mm (Wolotira, 1985), respectively, with enhanced swimming abilities that are difficult to capture in an IBM, thus fish larger than 45 mm in length were excluded from further analysis.

## 2.5. Data-model comparison with acoustic-trawl surveys

We used data on the abundance and length composition of larval (preflexion and flexion) and early juvenile polar cod and saffron cod (to 45 mm in length) from acoustic-trawl surveys conducted in the Chukchi Sea as part of the Arctic Eis program (Mueter et al., 2017) to compare with results from the IBMs developed in this study. In late summer 2012 and 2013, the Arctic Eis program conducted comprehensive ecosystem surveys of the U.S. northern Bering Sea and Chukchi Sea shelves (Mueter et al., 2017). Surveys began on 7 August in both years and progressed northward from Bering Strait along designated transects until reaching the Chukchi shelf break by the first week of September, after which sampling recommenced in Bering Strait and progressed southward to 60°N until the last week of September. Acoustic-trawl methods were used to estimate the abundance and distribution of pelagic organisms in the northern Bering and Chukchi seas (see De Robertis et al., 2017a, b for further details), and provide the best available information about the late summer distributions of age-0 polar cod and saffron cod in the region. The size and species composition of acoustic scatterers were estimated from a combination of surface trawls conducted at pre-determined stations and midwater trawls conducted in areas of high backscatter to convert the measurements of acoustic backscatter into animal abundances. A large Cantrawl rope trawl was used for all surface trawls and for midwater trawls in 2012, while a smaller modified-Marinovich trawl was used for midwater sampling in 2013. In 2013, a series of paired midwater trawls were conducted with the Cantrawl and modified-Marinovich trawls to determine the relative selectivity of the two gear types (De Robertis et al., 2017a). Selectivity-adjusted estimates of abundance (fish $m^{-2}$) for 10-mm size classes of polar cod and saffron cod ranging from 5 – 305 mm in length were calculated along the acoustic track.

Field distributions of polar cod and saffron cod were compared to simulated distributions by overlaying a 30- x 30-km grid over the 2012 and 2013 Arctic Eis acoustic-trawl survey areas

(Fig. S1) in ArcGIS (ESRI, 2017). Survey abundance estimates of fish ≤ 45 mm in length (all size classes ≤ 45 mm in length) were aggregated to each grid cell that overlapped with the survey area in each year. The aggregated abundance estimate for each cell was divided by the total survey abundance to get the proportion of the survey observations of fish ≤ 45 mm in length occurring in each grid cell. A similar process was used to determine the proportion of the simulated larvae falling within each survey grid cell for each release location and each hatch date. The locations of simulated polar cod and saffron cod ≤ 45 mm in length at the end of the simulation (1 September) were plotted and only those that overlapped with the survey grid cells were included in the analysis. The proportion of the simulated distribution that fell within each survey grid cell was calculated by dividing the number of simulated fish ≤ 45 mm in length occurring in each grid cell by the total number of simulated fish falling within the survey area. Note that we chose to analyze release locations and hatch dates separately, as aggregating larval releases over space and time assumes that each release location and time contributes equally, which is almost certainly not the case as the numbers of eggs released and the survival of larvae (which was not modeled) can be expected to vary widely across time and space. While the correlations between observed and simulated particles from a particular release location and time are not expected to be high when multiple hatching events contribute to larvae observed in a given region, significant correlations - even if weak - would strongly suggest that a given release location and time may have contributed to the observed concentrations of larvae.

Initial passive particle trajectory simulations from the northern release locations (Cape Lisburne, Hanna Shoal, and Barrow Canyon) showed poor overlap with the Arctic Ecosystem Integrated Survey (Arctic Eis) acoustic-trawl survey grids (see De Robertis et al., 2017b) used to ground truth the model (see Section 2.5 below), with most particles being advected into the Beaufort Sea and Arctic Basin (Fig. S2). Similarly, particles from the Norton Sound release location had minimal overlap with the acoustic-trawl survey grid and were largely retained in the Bering Sea (Fig. S2). Therefore, subsequent simulations were initialized from the five remaining locations with greater overlap with the acoustic-trawl surveys in 2012 and 2013 (i.e., transport into or retention within the Chukchi Sea), allowing for comparisons between simulated distributions and field observations.

Correlations between simulated distributions and survey observations were calculated for each behavior scenario, spawning location, release date, and release depth using Pearson's Product Moment Correlation, for a total of 525 comparisons per species per year. Correlations were consistent across release depths and are therefore reported for the total, depth-integrated values only.

500
501 **2.6. Interannual variability of simulated distributions**
502 To examine how polar cod and saffron cod dispersal were influenced by variability in
503 climate and oceanographic conditions, the IBMs were run for multiple years (2004 – 2015) over
504 the full range of hatch dates from the release areas that produced the strongest correlations
505 between observed and simulated distributions in 2012 and/or 2013. As simulations with surface-
506 oriented behavior showed the strongest correlations between observed and simulated distributions
507 for both species, this behaviour scenario was used to model polar cod and saffron cod dispersal
508 between 2004 and 2015.
509 Simulated distributions on 1 September from 2004 – 2015 were compared using a center
510 of gravity (COG) analysis in the R package SDMTools (R Core Team, 2018). Inertia, or the
511 dispersion of simulated particles around the COG (Woillez et al., 2009), was calculated for each
512 year, along with the standard deviations around the major and minor axes. This was done to test
513 for trends in spatial dispersion, which may reflect changes in oceanographic and atmospheric
514 circulation. For example, volume flow through Bering Strait has shown a strong, increasing trend
515 over recent years (Woodgate et al., 2015; Woodgate, 2018). Geographic coordinates (latitude,
516 longitude) were converted to projected coordinates using the North Pole Lambert Azimuthal
517 Equal Area (LAEA) Alaska projection (EPSG: 3572, https://epsg.io/3572, accessed 16
518 September, 2019) prior to the inertia calculation to minimize the distortion in lengths, areas, and
519 angles at the poles (Skopeliti and Tsoulos, 2013).
520
521 **2.7. Correlations with climate indices**
522 To examine how larval growth and connectivity may change under variable climate
523 forcing, we developed COG indices from the simulation output. Anomalies were calculated as
524 deviations from the mean latitude and longitude values for the 2004 – 2015 period normalized by
525 the standard deviation. Larval indices were then compared to several climate indices thought to
526 influence circulation in the Bering and Chukchi seas (Fig. S3). The large-scale climatic indices
527 selected were the winter (December – February) Arctic Oscillation (AO) index, which represents
528 the first empirical orthogonal function (EOF) pattern of sea level pressure (SLP) from 20 – 90°N
529 regressed to the SLP anomaly time series (Thompson and Wallace, 1998); the Arctic Dipole (AD)
530 index, which is the first EOF pattern of 70 – 90°N regressed to the SLP anomaly time series (Wu
531 et al., 2006); and the Siberian-Alaskan (SA) index, which provides a measure of atmospheric
532 circulation based on a correlation between sea ice cover and the 700 hPa geopotential height
533 gradient between Siberia and Alaska, that can be used to estimate thermal conditions in the

Bering Sea and ice cover extent (Overland et al., 2002). All indices were obtained from NOAA's Bering Climate website (https://www.beringclimate.noaa.gov/data/index.php, accessed 6 June, 2019).

An index representing ice extent and timing of retreat (IER) was developed for 2005 – 2015 based on the findings of Okkonen et al. (2019), where sea ice areal extent and concentration from April 1 through the third week of August were compared to late August water masses encountered during surveys in Barrow Canyon. Okkonen et al. (2019) found that greater daily sea ice extents and slower/later sea ice retreats occurred in years when the August late season meltwater (LMW) volumes in Barrow Canyon were greater than the 2005–2015 mean (2006, 2008, 2009, and 2012–2014; IER index = 1 in this study), while smaller daily sea ice extents and faster/earlier sea ice retreats occurred in years when August LMW volumes were less than the 2005–2015 mean (2005, 2007, 2010, 2011, and 2015; IER index = 0 in this study).

Correlations between the annual climate indices and the annual COG anomalies between 2004 and 2015 from the selected spawning/hatching areas were calculated for all hatch dates using Pearson's Product Moment Correlation. Correlations with the SA index were calculated for 2004 – 2013, as data beyond 2013 were not available. Similarly, correlations with the IER index were only calculated for 2005 – 2015, as 2004 data were not available. All statistical analyses were carried out in R (R Core Team, 2018).

## 3. Results

We found variations in simulated lengths-at-age between hatching areas and hatch dates for both polar cod and saffron cod. Overall, polar cod larvae that hatched from more southerly locations (Gulf of Anadyr, St. Lawrence Island), attained a greater length at the end of the simulation than those originating from the more northerly hatching locations (Fig. 4 a, b). This difference was more apparent in larvae hatched earlier in the year compared to those that hatched at later dates. Differences in length were also evident between years, with more variability in both simulated and observed polar cod lengths in 2013 compared to 2012 (Fig. 4 a, b). Saffron cod were much smaller in size at the end of the simulation than polar cod (Fig. 4) due to faster growth of polar cod at low temperatures (Fig. 2). While saffron cod lengths differed between southerly and northerly hatching locations, the difference was not as great as that found for polar cod, again, likely due to slower growth of saffron cod at low temperatures. The difference in length remained fairly consistent across hatch dates in 2012, but was less apparent in 2013 (Fig. 4 c, d). Despite some overlap, simulated sizes based on lab-derived growth were smaller than the sizes

observed in the Arctic Eis acoustic-trawl survey (Fig. 4). This overlap was much greater for polar cod and nearly absent for saffron cod (Fig. 4).

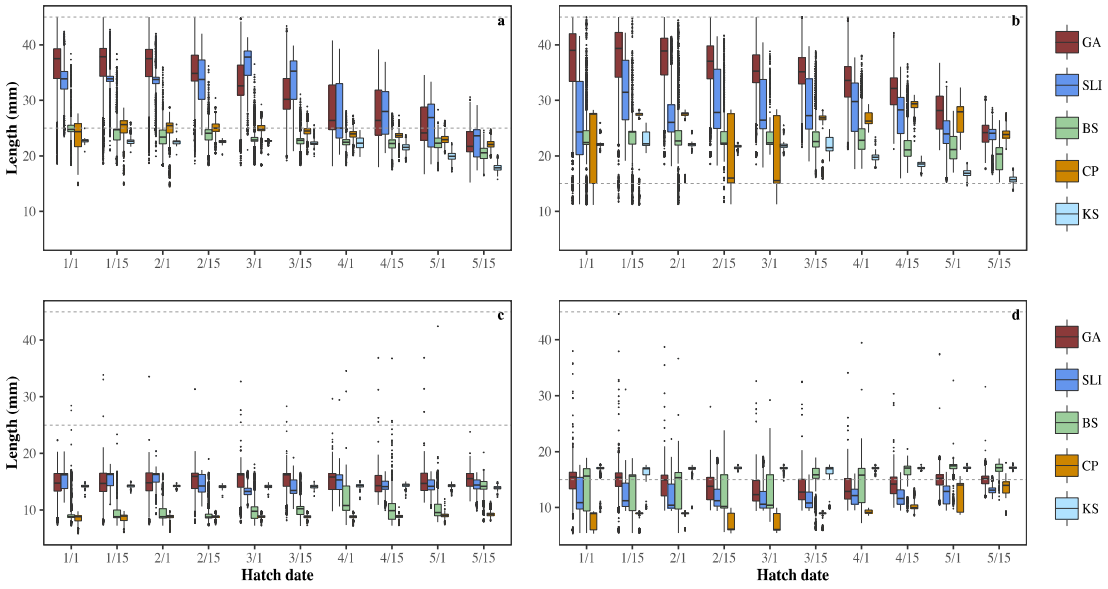


Fig. 4. Simulated lengths of (a, b) polar cod (*Boreogadus saida*) and (c, d) saffron cod (*Eleginus gracilis*) larvae and early juveniles ≤ 45 mm in length located within the Arctic Ecosystem Integrated Survey acoustic-trawl survey area on 1 September (a, c) 2012 and (b, d) 2013. Simulations were initiated from five hypothesized areas on 10 hatch dates. Data presented are from simulations with surface-oriented behavior, which had the strongest correlations with the acoustic-trawl survey data. The dashed grey lines represent the minimum and maximum lengths estimated by the survey (to 45 mm). GA: Gulf of Anadyr; SLI: St. Lawrence Island; BS: Bering Strait; CP: Chukotka Peninsula; KS: Kotzebue Sound. The minimum, first quartile (Q1), median, third quartile (Q3), maximum, and outliers are represented.

### 3.1. Data-model comparison with acoustic-trawl surveys

We found distinct differences in larval distributions between the different behavior scenarios, particularly for those simulations with a passive component (Fig. S4). Behavior scenarios that included a surface component produced relatively similar distributions, especially for the simulations with and without DVM for surface-oriented early larvae that moved deeper with ontogeny, which had almost identical distributions (Fig. S4, Tables 3 and 4). Simulated and observed polar cod larval distributions were not significantly correlated for any of the hatching locations in 2012, except for larvae with surface-oriented behavior that were released around

Bering Strait and the Chukotka Peninsula (Table 3). Significant positive correlations were also found for simulations from the Chukotka Peninsula with all other behavioral scenarios except that with DVM (Table 3). Earlier hatching larvae resulted in significant overlap with observed distributions from the Bering Strait release location, while the correlations for the Chukotka Peninsula simulations were significant across all release dates (Table 3). No significant correlations were found between observed and simulated distributions of polar cod in 2013 (not shown).

Table 3. Correlations between observed distributions of polar cod (*Boreogadus saida*, larvae and early juveniles ≤ 45 mm in length) in the 2012 Arctic Ecosystem Integrated Survey acoustic-trawl survey and simulated distributions on 1 September from 5 different behavior scenarios. Particles were released at 5 locations (Gulf of Anadyr, St. Lawrence Island, Bering Strait, Chukotka Peninsula, and Kotzebue Sound) on the 1st and 15th of each month from 1 January – 15 May. **$p$-value < 0.05 (darker shading), *0.05 ≤ $p$-value < 0.10 (lighter shading). $p$ = p-value, n = number of simulated larvae found within the survey grid.

| **Gulf of Anadyr** | **1-Jan** | | **15-Jan** | | **1-Feb** | | **15-Feb** | | **1-Mar** | | **15-Mar** | | **1-Apr** | | **15-Apr** | | **1-May** | | **15-May** | |
|---|---|---|---|---|---|---|---|---|---|---|---|---|---|---|---|---|---|---|---|---|
| | ***p*** | **n** | ***p*** | **n** | ***p*** | **n** | ***p*** | **n** | ***p*** | **n** | ***p*** | **n** | ***p*** | **n** | ***p*** | **n** | ***p*** | **n** | ***p*** | **n** |
| Passive | 0.03 | 91,390 | 0.03 | 91,163 | 0.02 | 94,815 | 0.01 | 104,614 | -0.01 | 105,849 | -0.02 | 109,275 | -0.04 | 103,251 | -0.04 | 97,109 | -0.06 | 101,004 | -0.07 | 100,556 |
| Surface | -0.02 | 38,155 | -0.02 | 40,114 | -0.02 | 44,571 | -0.02 | 62,964 | -0.02 | 80,874 | -0.02 | 84,324 | -0.02 | 73,119 | -0.02 | 57,679 | -0.02 | 51,354 | 0.69 | 43,574 |
| Passive - ontogeny | -0.02 | 50,958 | -0.03 | 41,543 | -0.02 | 50,757 | -0.02 | 56,645 | -0.02 | 67,049 | -0.02 | 62,470 | -0.02 | 26,115 | -0.02 | 48,579 | -0.02 | 26,971 | -0.02 | 15,931 |
| Surface - ontogeny | -0.02 | 52,411 | -0.02 | 53,259 | -0.02 | 52,891 | -0.02 | 62,469 | -0.02 | 73,683 | -0.02 | 79,238 | -0.02 | 76,250 | -0.02 | 55,023 | -0.02 | 39,206 | -0.02 | 45,681 |
| Surface - DVM | -0.02 | 59,301 | -0.02 | 59,764 | -0.02 | 53,148 | -0.02 | 65,007 | -0.02 | 77,822 | -0.02 | 82,680 | -0.02 | 78,528 | -0.02 | 56,045 | -0.02 | 38,677 | -0.02 | 46,336 |
| **St. Lawrence Island** | **1-Jan** | | **15-Jan** | | **1-Feb** | | **15-Feb** | | **1-Mar** | | **15-Mar** | | **1-Apr** | | **15-Apr** | | **1-May** | | **15-May** | |
| Passive | -0.06 | 5,791 | -0.03 | 5,495 | -0.03 | 5,348 | -0.04 | 5,149 | -0.02 | 5,172 | -0.01 | 5,720 | 0.07 | 3,976 | -0.10 | 6,569 | -0.10 | 5,379 | -0.08 | 5,677 |
| Surface | -0.02 | 3,581 | -0.02 | 4,871 | -0.02 | 5,217 | -0.03 | 3,488 | -0.05 | 2,545 | -0.05 | 3,493 | -0.03 | 4,861 | -0.04 | 5,477 | -0.04 | 5,467 | -0.04 | 6,990 |
| Passive - ontogeny | -0.02 | 3,355 | -0.02 | 3,941 | -0.02 | 2,879 | -0.03 | 1,989 | -0.03 | 145 | -0.02 | 892 | -0.03 | 4,461 | -0.04 | 4,947 | -0.05 | 3,734 | -0.05 | 4,644 |
| Surface - ontogeny | -0.02 | 4,246 | -0.02 | 4,889 | -0.02 | 4,015 | -0.02 | 3,175 | -0.04 | 1,569 | -0.03 | 2,197 | -0.03 | 6,100 | -0.04 | 5,721 | -0.04 | 4,738 | -0.03 | 6,584 |
| Surface - DVM | -0.02 | 4,528 | -0.02 | 5,164 | -0.02 | 3,581 | -0.03 | 3,647 | -0.05 | 2,427 | -0.04 | 2,831 | -0.03 | 6,062 | -0.04 | 5,859 | -0.04 | 4,781 | -0.03 | 6,595 |
| **Bering Strait** | **1-Jan** | | **15-Jan** | | **1-Feb** | | **15-Feb** | | **1-Mar** | | **15-Mar** | | **1-Apr** | | **15-Apr** | | **1-May** | | **15-May** | |
| Passive | 0.03 | 11,921 | 0.04 | 12,022 | 0.04 | 11,877 | 0.05 | 12,561 | 0.06 | 12,373 | 0.05 | 12,948 | 0.05 | 16,310 | 0.10 | 16,948 | 0.07 | 16,368 | 0.06 | 20,114 |
| Surface | 0.30** | 14,816 | 0.22** | 11,223 | 0.12* | 7,934 | 0.26** | 9,829 | 0.01 | 9,549 | 0.01 | 7,615 | 0.00 | 15,331 | 0.03 | 16,121 | 0.01 | 18,374 | -0.03 | 6,406 |
| Passive - ontogeny | 0.05 | 15,473 | -0.01 | 14,627 | 0.02 | 14,611 | -0.02 | 11,453 | 0.01 | 8,606 | 0.05 | 11,894 | 0.02 | 13,646 | -0.01 | 8,174 | 0.07 | 11,164 | -0.01 | 7,293 |
| Surface - ontogeny | 0.05 | 17,142 | 0.06 | 15,190 | 0.05 | 12,913 | 0.06 | 15,923 | 0.04 | 18,346 | 0.06 | 18,840 | 0.03 | 19,417 | 0.06 | 22,183 | 0.04 | 13,247 | -0.02 | 20,114 |
| Surface - DVM | 0.05 | 16,772 | 0.06 | 15,186 | 0.05 | 12,913 | 0.06 | 15,914 | 0.04 | 18,337 | 0.06 | 18,830 | 0.03 | 19,419 | 0.06 | 22,214 | 0.04 | 13,250 | -0.02 | 6,632 |
| **Chukotka Peninsula** | **1-Jan** | | **15-Jan** | | **1-Feb** | | **15-Feb** | | **1-Mar** | | **15-Mar** | | **1-Apr** | | **15-Apr** | | **1-May** | | **15-May** | |
| Passive | 0.02 | 9,231 | 0.04 | 9,526 | 0.03 | 8,877 | 0.06 | 9,115 | 0.06 | 10,106 | 0.05 | 10,763 | 0.03 | 13,869 | 0.06 | 16,530 | 0.11 | 20,238 | 0.18** | 20,943 |
| Surface | 0.20** | 6,801 | 0.27** | 5,390 | 0.24** | 6,904 | 0.30** | 6,749 | 0.45** | 10,653 | 0.38** | 11,016 | 0.29** | 12,042 | 0.47** | 6,867 | 0.24** | 9,976 | 0.12* | 13,498 |
| Passive - ontogeny | 0.18** | 18,590 | 0.09 | 13,126 | 0.10 | 11,698 | 0.06 | 12,930 | 0.06 | 3,933 | 0.07 | 4,964 | 0.10 | 14,398 | 0.00 | 4,611 | 0.01 | 877 | 0.13* | 10,356 |
| Surface - ontogeny | 0.06 | 4,189 | 0.11 | 6,800 | 0.06 | 7,967 | 0.06 | 4,789 | 0.01 | 7,755 | 0.05 | 13,860 | 0.04 | 18,649 | 0.15** | 10,708 | 0.16* | 9,084 | 0.12* | 10,836 |
| Surface - DVM | 0.05 | 4,189 | 0.06 | 6,804 | 0.05 | 7,968 | 0.06 | 4,801 | 0.04 | 7,747 | 0.06 | 13,874 | 0.03 | 18,674 | 0.06 | 10,689 | 0.04 | 9,078 | -0.02 | 10,836 |
| **Kotzebue Sound** | **1-Jan** | | **15-Jan** | | **1-Feb** | | **15-Feb** | | **1-Mar** | | **15-Mar** | | **1-Apr** | | **15-Apr** | | **1-May** | | **15-May** | |
| Passive | 0.07 | 2,983 | 0.10 | 2,990 | 0.11* | 2,914 | 0.09 | 3,013 | 0.09 | 3,762 | 0.07 | 3,976 | 0.06 | 3,893 | 0.05 | 4,366 | 0.04 | 4,764 | 0.13* | 4,571 |
| Surface | -0.02 | 1,056 | -0.02 | 1,200 | -0.02 | 1,379 | -0.01 | 956 | -0.02 | 1,006 | -0.02 | 1,272 | -0.02 | 1,992 | -0.02 | 3,806 | -0.02 | 2,793 | -0.02 | 1,391 |
| Passive - ontogeny | -0.02 | 1,006 | -0.02 | 3,858 | -0.02 | 3,270 | -0.02 | 1,637 | -0.02 | 2,842 | 0.01 | 2,643 | 0.00 | 2,463 | -0.02 | 433 | -0.02 | 1,783 | -0.02 | 2,361 |
| Surface - ontogeny | -0.02 | 1,042 | -0.02 | 1,008 | -0.02 | 1,457 | -0.02 | 1,129 | -0.02 | 1,188 | -0.02 | 1,391 | -0.02 | 2,173 | -0.02 | 4,261 | -0.02 | 3,221 | -0.02 | 1,514 |
| Surface - DVM | -0.02 | 1,042 | -0.02 | 1,008 | -0.02 | 1,457 | -0.02 | 1,129 | -0.02 | 1,188 | -0.02 | 1,393 | -0.02 | 2,173 | -0.02 | 4,261 | -0.02 | 3,221 | -0.02 | 1,514 |

For saffron cod, the simulations that produced results most similar to observed field distributions in 2012 were those initiated from Bering Strait and Kotzebue Sound. Simulations

610 initiated from Bering Strait were significantly correlated for all simulation behaviors across most
611 simulation dates, while those initiated from Kotzebue Sound were significant across all behaviors
612 and dates (Table 4). Early passive particle simulations from the Chukotka Peninsula (15 January
613 – 1 March) were also marginally or significantly correlated with observations (Table 4). No
614 significant correlations were found for other release locations. Similar to the 2012 results, most
615 simulations in 2013 from Bering Strait and Kotzebue Sound produced distributions that were
616 significantly correlated to observed distributions of saffron cod in the acoustic-trawl survey (not
617 shown). For both 2012 and 2013 simulations, the majority of correlations were strongest for later
618 release dates (Table 4 for 2012, not shown for 2013). Correlations with release depth did not
619 reveal any patterns for either species, except for saffron cod simulations initiated in Kotzebue
620 Sound, where correlations were significant for all release depths across all behaviors (not shown).
621 Note that most release dates occurred in winter and spring months, when the shallow Chukchi and
622 Bering shelf water columns exhibit relatively weak stratification. Hence, current-induced
623 turbulent motions can readily redistribute passively floating plankton through the water column at
624 this time of year.
625
626 Table 4. Correlations between observed distributions of saffron cod (*Eleginus gracilis*, larvae and
627 early juveniles ≤ 45 mm in length) in the 2012 Arctic Ecosystem Integrated Survey acoustic-trawl
628 survey and simulated distributions on 1 September from 5 behavior scenarios. Particles were
629 released at 5 locations (Gulf of Anadyr, St. Lawrence Island, Bering Strait, Chukotka Peninsula,
630 and Kotzebue Sound) at bi-weekly intervals from 1 January – 15 May. ***p*-value < 0.05 (darker
631 shading), *0.05 ≤ *p*-value < 0.10 (lighter shading). *p* = p-value, n = number of simulated larvae
632 found within the survey grid.

| Gulf of Anadyr | 1-Jan | | 15-Jan | | 1-Feb | | 15-Feb | | 1-Mar | | 15-Mar | | 1-Apr | | 15-Apr | | 1-May | | 15-May | |
|---|---|---|---|---|---|---|---|---|---|---|---|---|---|---|---|---|---|---|---|---|
| | *p* | n | *p* | n | *p* | n | *p* | n | *p* | n | *p* | n | *p* | n | *p* | n | *p* | n | *p* | n |
| Passive | 0.09 | 93,331 | 0.07 | 93,269 | 0.05 | 96,398 | 0.03 | 105,121 | 0.02 | 105,953 | 0.02 | 109,282 | 0.01 | 103,251 | 0.01 | 97,108 | 0.01 | 101,002 | -0.01 | 100,556 |
| Surface | -0.01 | 43,457 | 0.01 | 45,721 | -0.02 | 49,470 | -0.02 | 66,645 | -0.02 | 79,270 | -0.01 | 82,426 | -0.01 | 72,419 | -0.02 | 56,892 | -0.02 | 50,650 | -0.02 | 43,385 |
| Passive - ontogeny | -0.01 | 54,753 | -0.01 | 41,934 | -0.01 | 60,111 | -0.01 | 79,601 | -0.01 | 88,225 | -0.01 | 80,818 | -0.01 | 77,832 | -0.01 | 82,431 | -0.01 | 30,342 | -0.01 | 27,890 |
| Surface - ontogeny | -0.01 | 44,123 | -0.01 | 46,344 | -0.01 | 49,833 | -0.02 | 67,621 | -0.02 | 80,369 | -0.01 | 83,384 | -0.01 | 71,798 | -0.02 | 57,966 | -0.02 | 50,017 | -0.02 | 40,788 |
| Surface - DVM | -0.01 | 43,821 | -0.01 | 46,173 | -0.01 | 52,891 | -0.02 | 67,924 | -0.02 | 80,535 | -0.01 | 83,070 | -0.01 | 71,566 | -0.02 | 57,810 | -0.02 | 50,138 | -0.02 | 40,622 |
| **St. Lawrence Island** | **1-Jan** | | **15-Jan** | | **1-Feb** | | **15-Feb** | | **1-Mar** | | **15-Mar** | | **1-Apr** | | **15-Apr** | | **1-May** | | **15-May** | |
| Passive | -0.03 | 5,861 | -0.01 | 5,549 | 0.08 | 5,349 | -0.01 | 5,149 | -0.02 | 5,172 | 0.00 | 5,720 | -0.05 | 5,654 | -0.05 | 6,569 | -0.05 | 5,379 | -0.04 | 5,677 |
| Surface | -0.02 | 3,565 | -0.02 | 4,957 | -0.01 | 5,315 | -0.02 | 3,364 | -0.04 | 2,478 | -0.03 | 3,393 | -0.02 | 4,836 | -0.03 | 5,502 | -0.03 | 5,440 | -0.03 | 6,971 |
| Passive - ontogeny | -0.01 | 2,047 | -0.01 | 830 | -0.01 | 1,963 | -0.01 | 194 | -0.03 | 2,394 | -0.02 | 1,007 | -0.02 | 6,967 | -0.03 | 5,076 | -0.04 | 3,643 | -0.03 | 5,685 |
| Surface - ontogeny | -0.02 | 3,574 | -0.01 | 5,005 | -0.01 | 5,360 | -0.02 | 3,361 | -0.03 | 2,401 | -0.03 | 3,205 | -0.02 | 5,126 | -0.02 | 5,772 | -0.03 | 5,017 | -0.02 | 6,484 |
| Surface - DVM | -0.02 | 4,246 | -0.01 | 4,889 | -0.01 | 4,015 | -0.02 | 3,175 | -0.03 | 2,398 | -0.03 | 3,205 | -0.02 | 5,132 | -0.02 | 5,772 | -0.03 | 5,017 | -0.02 | 6,484 |
| **Bering Strait** | **1-Jan** | | **15-Jan** | | **1-Feb** | | **15-Feb** | | **1-Mar** | | **15-Mar** | | **1-Apr** | | **15-Apr** | | **1-May** | | **15-May** | |
| Passive | 0.48** | 11,924 | 0.46** | 12,032 | 0.46** | 11,877 | 0.44** | 12,561 | 0.55** | 12,373 | 0.53** | 12,947 | 0.59** | 16,310 | 0.47** | 16,948 | 0.51** | 16,368 | 0.81** | 20,114 |
| Surface | 0.05 | 15,665 | 0.21** | 12,008 | 0.18** | 7,799 | 0.12* | 9,881 | 0.07 | 9,538 | 0.09 | 7,558 | 0.54** | 15,149 | 0.17** | 15,947 | 0.06 | 18,153 | 0.54** | 6,223 |
| Passive - ontogeny | 0.13** | 12,915 | 0.07 | 12,416 | 0.27** | 11,276 | 0.42** | 9,716 | 0.35** | 13,438 | 0.30** | 20,259 | 0.56** | 15,592 | 0.19** | 16,878 | 0.22** | 11,819 | 0.72** | 7,840 |
| Surface - ontogeny | 0.05 | 15,699 | 0.24** | 12,221 | 0.20** | 8,005 | 0.14** | 10,027 | 0.08 | 9,670 | 0.10 | 7,684 | 0.56** | 15,620 | 0.19** | 16,207 | 0.07 | 18,284 | 0.59** | 6,512 |
| Surface - DVM | 0.31** | 17,142 | 0.25** | 15,190 | 0.06 | 12,913 | 0.06 | 15,923 | 0.02 | 18,346 | 0.11 | 7,725 | 0.56** | 15,666 | 0.19** | 16,170 | 0.07 | 18,249 | 0.59** | 6,512 |
| **Chukotka Peninsula** | **1-Jan** | | **15-Jan** | | **1-Feb** | | **15-Feb** | | **1-Mar** | | **15-Mar** | | **1-Apr** | | **15-Apr** | | **1-May** | | **15-May** | |
| Passive | 0.10 | 9,231 | 0.12* | 9,526 | 0.13** | 8,877 | 0.10 | 9,115 | 0.11** | 10,106 | 0.10 | 10,763 | 0.10 | 13,869 | 0.08 | 16,529 | 0.07 | 20,238 | 0.05 | 20,943 |
| Surface | -0.04 | 7,192 | -0.04 | 4,857 | -0.04 | 7,347 | -0.03 | 6,789 | -0.03 | 10,632 | -0.03 | 10,912 | -0.03 | 11,935 | -0.03 | 6,855 | -0.02 | 9,851 | -0.02 | 13,471 |
| Passive - ontogeny | -0.04 | 4,321 | -0.03 | 11,390 | -0.05 | 773 | -0.03 | 12,264 | -0.02 | 2,286 | -0.03 | 16,980 | -0.04 | 12,078 | -0.03 | 6,527 | -0.02 | 10,829 | -0.04 | 1,088 |
| Surface - ontogeny | -0.04 | 7,249 | -0.04 | 4,889 | -0.04 | 7,424 | -0.03 | 6,818 | -0.03 | 10,662 | -0.03 | 10,938 | -0.03 | 12,021 | -0.03 | 6,946 | -0.02 | 9,809 | -0.02 | 13,501 |
| Surface - DVM | -0.02 | 4,189 | -0.03 | 6,800 | -0.03 | 7,967 | -0.03 | 4,789 | -0.03 | 7,755 | -0.03 | 11,012 | -0.03 | 12,061 | -0.03 | 6,935 | -0.02 | 9,820 | -0.02 | 13,452 |
| **Kotzebue Sound** | **1-Jan** | | **15-Jan** | | **1-Feb** | | **15-Feb** | | **1-Mar** | | **15-Mar** | | **1-Apr** | | **15-Apr** | | **1-May** | | **15-May** | |
| Passive | 0.34** | 2,983 | 0.33** | 2,990 | 0.34** | 2,914 | 0.57** | 3,013 | 0.65** | 3,762 | 0.67** | 3,975 | 0.68** | 3,893 | 0.78** | 4,366 | 0.81** | 4,764 | 0.77** | 4,571 |
| Surface | 0.22** | 1,068 | 0.35** | 1,201 | 0.22** | 1,387 | 0.22** | 982 | 0.22** | 1,023 | 0.28** | 1,265 | 0.71** | 1,953 | 0.75** | 3,763 | 0.76** | 2,720 | 0.41** | 1,399 |
| Passive - ontogeny | 0.76** | 1,097 | 0.75** | 2,636 | 0.76** | 4,678 | 0.45** | 1,648 | 0.76** | 3,664 | 0.27** | 2,970 | 0.70** | 2,979 | 0.41** | 1,106 | 0.63** | 2,453 | 0.41** | 1,953 |
| Surface - ontogeny | 0.22** | 1,072 | 0.34** | 1,201 | 0.22** | 1,396 | 0.22** | 966 | 0.22** | 1,029 | 0.29** | 1,291 | 0.72** | 2,054 | 0.75** | 4,069 | 0.76** | 3,032 | 0.45** | 1,469 |
| Surface - DVM | 0.22** | 1,042 | 0.34** | 1,008 | 0.24** | 1,457 | 0.22** | 1,129 | 0.26** | 1,188 | 0.30** | 1,293 | 0.72** | 2,057 | 0.75** | 4,061 | 0.76** | 3,035 | 0.45** | 1,465 |

### 3.2. Interannual variability in simulated distributions

Large interannual variability in the COGs of simulated particles was found for polar cod, particularly for the Chukotka Peninsula release locations. The COG across simulation years (2004 – 2015) was located in the western portion of the Chukchi Sea, southwest of Herald Shoal (Fig. 5 a), similar to the centers of gravity in 2008, 2013, and 2015. For 2004 – 2006, the COGs shifted to the southwest, while that in 2012 was to the southeast (Fig. 5 a). In 2007, 2011, and 2014, particles were located further north compared to the 2004 – 2015 COG. In 2009, the COG was in the eastern portion of the Chukchi Sea, east of Herald Shoal, while in 2010, it was in the western Chukchi Sea, just south of Wrangel Island (Fig. 5 a). Most of the COGs for the Bering Strait release location were found in close proximity to Cape Lisburne, located north and south of the cape for the majority of the time series. The only exceptions were in 2005, when the COG was located near Herald Shoal, and in 2007, when it was farther north of Cape Lisburne compared to in other years (Fig. 4 a). The COGs of saffron cod released from the Bering Strait region were similar to those of polar cod and were mainly centered around Cape Lisburne (Fig. 5 b). In 2005, the COG was over Herald Shoal, while in 2007 it was located to the north of Cape Lisburne (Fig. 5 b). The COGs for particles released in Kotzebue Sound were found on the north side of the sound, located around Cape Krusenstern (Fig. 5 b), suggesting retention within Kotzebue Sound.

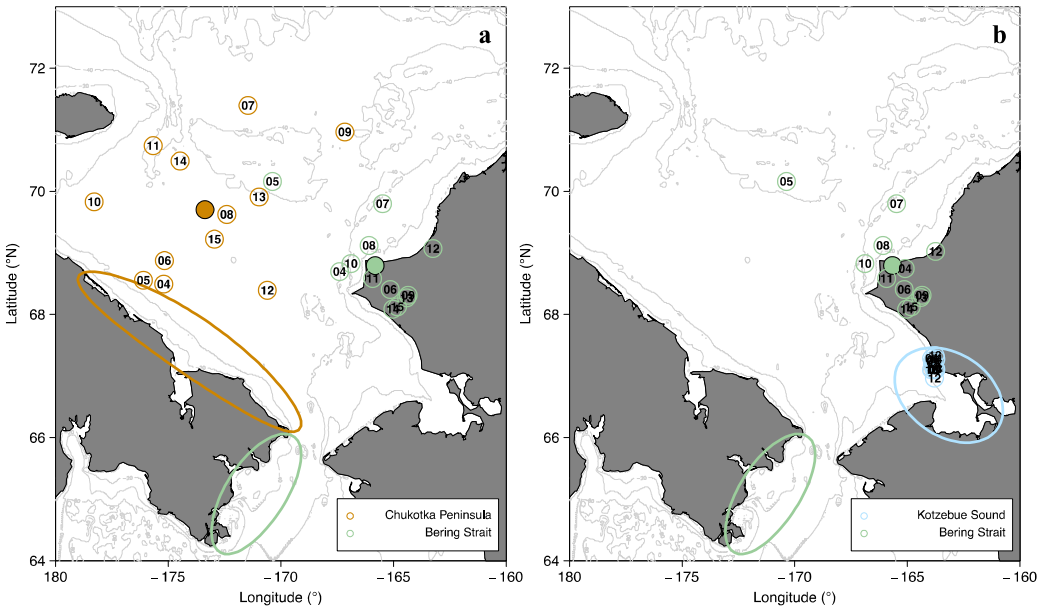


Fig. 5. Mean latitude and longitude of (a) polar cod (*Boreogadus saida*) and (b) saffron cod (*Eleginus gracilis*) larvae and early juveniles ≤ 45 mm in length on 1 September from 2004 – 2015. Simulations for polar cod were initiated from Bering Strait (green) and the Chukotka Peninsula (orange). Simulations for saffron cod were initiated from Bering Strait (green) and Kotzebue Sound (blue). Data from simulations with surface-oriented behavior are presented. Solid circles represent overall centers of gravity for 2004 – 2015, color coded to release location. Numbers in circles represent the last two digits of the simulation year. Ellipses represent particle release locations.

Polar cod inertia between 2004 and 2015 was highly variable for both the Bering Strait and Chukotka Peninsula simulations (Fig. 6). Bering Strait had a mean inertia of 97,755 km$^2$ and a SD of the major and minor axes of ± 260,074 km$^2$ and ± 173,542 km$^2$, respectively. The Chukotka Peninsula had a mean inertia of 123,034 km$^2$ and a SD of the major and minor axes of ± 283,059 km$^2$ and ± 207,150 km$^2$, respectively. For Bering Strait releases, inertia declined significantly over time (linear regression, LR: $\beta$ = -5894, $t_{10}$ = -3.129, $p$ = 0.011), while it increased over time for simulations originating from the Chukotka Peninsula, although not significantly (LR: $\beta$ = 4914, $t_{10}$ = 1.568, $p$ = 0.148). Similar to polar cod, saffron cod inertia for the Bering Strait release location was highly variable (95,729 ± 261,437 and 165,469 km$^2$) and declined significantly over time (LR: $\beta$ = -5044, $t_{10}$ = -2.611, $p$ =0.026). Inertia for simulations

originating in Kotzebue Sound was very low (15, 475 ± 115,195 and 46,956 km$^2$) and remained relatively constant over time (LR: $\beta$ = -106.2, $t_{10}$ = -0.384, $p$ = 0.709).

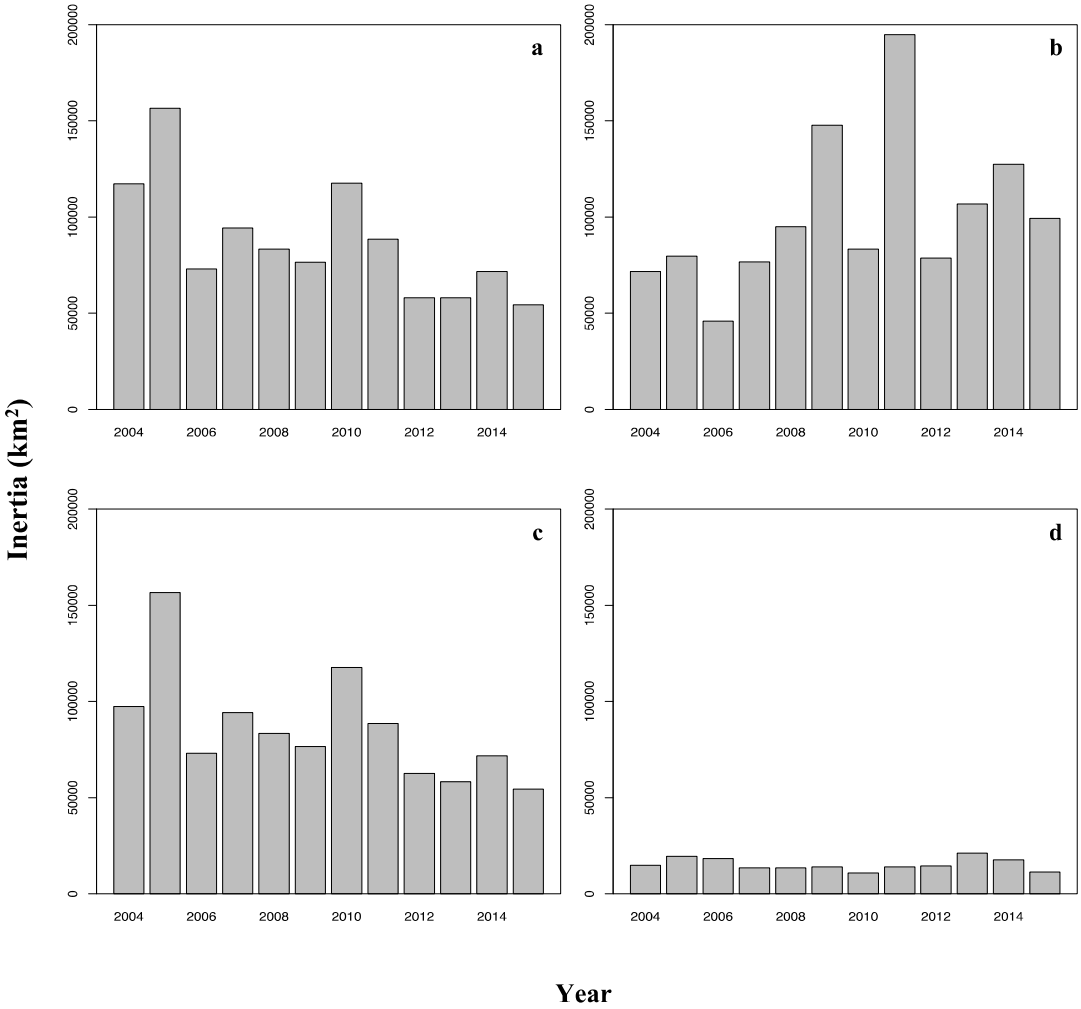


Fig. 6. Inertia (in km$^2$), which measures the dispersion of simulated particles around the center of gravity, for polar cod (*Boreogadus saida*) simulations from (a) Bering Strait and the (b) Chukotka Peninsula and saffron cod (*Eleginus gracilis*) simulations from (c) Bering Strait and (d) Kotzebue Sound from 2004 – 2015. Data from simulations with surface-oriented behavior are presented.

### 3.3. Correlations with climate indices

Significant correlations were found between latitudinal and longitudinal COG indices for both polar cod and saffron cod at the end of the simulation and several of the climate indices, although correlations were not consistent across release areas or dates (Tables 5, 6). Simulated

687 particles from the Bering Strait region for both species tended to have a more southern and
688 eastern COG during years with a strong summer AD index, a weaker SA index, and more
689 extensive ice (IER index = 1). In most cases, these correlations were stronger for later release
690 dates (March – May). Similarly, the COG of simulated polar cod released at the Chukotka
691 Peninsula were further south and east when the summer AD and AO indices were high and ice
692 was extensive and retreated later (IER index = 1). In contrast to Bering Strait releases, the COG
693 of simulated particles from the Chukotka Peninsula, in particular early releases, occurred further
694 south during years with a stronger SA index, as evidenced by negative correlations with latitude
695 (Table 5). For saffron cod from the Kotzebue Sound release locations, environmental variability
696 appeared to primarily affect the longitudinal COG of early releases but the latitudinal COG from
697 later releases. Simulated particles from earlier release dates were displaced to the east during
698 years with stronger AO and SA indices and a weaker winter AD index, all indicative of cold
699 winters with heavy ice. Correlations with the latitudinal COG were variable and inconsistent
700 (Table 6).
701
702 Table 5. Correlations between latitude and longitude center of gravity (COG) anomalies of
703 simulated polar cod (*Boreogadus saida*, larvae and early juveniles ≤ 45 mm in length) on 1
704 September (2004 – 2015) and selected climate indices. AD: Arctic Dipole index, MAM: March,
705 April, May, JJA: June, July, August; AO: Arctic Oscillation index; SA: Siberian/Alaskan index
706 (2004 – 2013); IER: Ice extent/retreat index (2005 – 2015). Simulations were initiated from
707 Bering Strait and Chukotka Peninsula release locations using surface-oriented behavior. **$p$-
708 value < 0.05 (darker shading), *0.05 ≤ $p$-value < 0.10 (lighter shading). Red (blue) represents a
709 positive (negative) correlation.
710
711

| Bering Strait | | | | | | Chukotka Peninsula | | | | | |
|---|---|---|---|---|---|---|---|---|---|---|---|
| **Latitude COG Index** | **AD (MAM)** | **AD (JJA)** | **AO** | **SA** | **IER** | **Latitude COG Index** | **AD (MAM)** | **AD (JJA)** | **AO** | **SA** | **IER** |
| Lat, all dates | -0.12 | -0.22 | 0.16 | 0.39 | -0.42 | Lat, all dates | 0.13 | -0.60** | 0.07 | -0.37 | -0.12 |
| Lat, 1-Jan | -0.23 | 0.19 | -0.12 | -0.06 | -0.43 | Lat, 1-Jan | 0.16 | -0.29 | -0.42 | -0.47 | -0.28 |
| Lat, 15-Jan | -0.08 | 0.21 | -0.08 | -0.10 | -0.19 | Lat, 15-Jan | -0.04 | -0.36 | -0.20 | -0.24 | 0.07 |
| Lat, 1-Feb | -0.22 | 0.25 | -0.11 | 0.00 | 0.00 | Lat, 1-Feb | 0.14 | -0.53* | -0.01 | -0.37 | -0.06 |
| Lat, 15-Feb | 0.00 | 0.02 | 0.07 | 0.45 | -0.28 | Lat, 15-Feb | 0.27 | -0.44 | -0.16 | -0.54 | -0.01 |
| Lat, 1-Mar | 0.26 | -0.32 | 0.16 | 0.16 | -0.55* | Lat, 1-Mar | 0.16 | -0.50* | -0.15 | -0.58* | -0.05 |
| Lat, 15-Mar | -0.01 | -0.32 | 0.51* | 0.58* | -0.24 | Lat, 15-Mar | 0.00 | -0.64** | -0.12 | -0.49 | -0.25 |
| Lat, 1-Apr | -0.31 | -0.66** | 0.44 | 0.40 | 0.00 | Lat, 1-Apr | -0.08 | -0.66** | 0.43 | -0.18 | 0.18 |
| Lat, 15-Apr | -0.11 | -0.64** | 0.02 | 0.30 | -0.53* | Lat, 15-Apr | -0.13 | -0.42 | 0.45 | 0.18 | -0.37 |
| Lat, 1-May | -0.15 | -0.38 | 0.37 | 0.87** | 0.05 | Lat, 1-May | 0.23 | -0.46 | 0.49 | -0.04 | -0.15 |
| Lat, 15-May | 0.15 | -0.33 | 0.13 | 0.32 | -0.77** | Lat, 15-May | 0.17 | -0.36 | 0.54* | 0.07 | -0.10 |
| **Longitude COG Index** | **AD (MAM)** | **AD (JJA)** | **AO** | **SA** | **IER** | **Longitude COG Index** | **AD (MAM)** | **AD (JJA)** | **AO** | **SA** | **IER** |
| Lon, all dates | 0.15 | 0.06 | 0.17 | 0.18 | 0.56* | Lon, all dates | -0.13 | -0.10 | 0.61** | 0.09 | 0.52 |
| Lon, 1-Jan | -0.08 | 0.34 | 0.55* | 0.13 | 0.42 | Lon, 1-Jan | -0.29 | -0.24 | 0.63** | 0.13 | 0.33 |
| Lon, 15-Jan | 0.20 | 0.12 | -0.19 | -0.03 | 0.42 | Lon, 15-Jan | -0.13 | -0.26 | 0.54* | -0.10 | 0.27 |
| Lon, 1-Feb | 0.36 | 0.03 | 0.16 | 0.13 | 0.39 | Lon, 1-Feb | 0.04 | -0.36 | 0.48 | -0.06 | 0.36 |
| Lon, 15-Feb | 0.41 | 0.06 | -0.02 | 0.10 | 0.31 | Lon, 15-Feb | 0.16 | -0.09 | 0.28 | -0.17 | 0.45 |
| Lon, 1-Mar | 0.13 | 0.26 | 0.10 | 0.13 | 0.72** | Lon, 1-Mar | -0.05 | 0.08 | 0.32 | -0.06 | 0.63** |
| Lon, 15 Mar | -0.25 | 0.12 | 0.12 | 0.42 | 0.72** | Lon, 15 Mar | -0.20 | -0.11 | 0.49 | 0.14 | 0.67** |
| Lon, 1-Apr | 0.03 | -0.12 | 0.14 | 0.10 | 0.50 | Lon, 1-Apr | -0.09 | -0.04 | 0.46 | 0.16 | 0.54* |
| Lon, 15-Apr | 0.02 | -0.10 | 0.50* | 0.24 | 0.50 | Lon, 15-Apr | -0.30 | 0.17 | 0.56* | 0.52 | 0.35 |
| Lon, 1-May | 0.12 | -0.12 | 0.02 | 0.36 | 0.37 | Lon, 1-May | -0.02 | 0.03 | 0.56* | 0.14 | 0.27 |
| Lon, 15-May | 0.38 | 0.01 | -0.26 | 0.02 | 0.37 | Lon, 15-May | 0.03 | 0.09 | 0.54* | 0.11 | 0.26 |

Table 6. Correlations between latitude and longitude center of gravity (COG) anomalies of simulated saffron cod (*Eleginus gracilis*, larvae and early juveniles ≤ 45 mm in length) on 1 September (2004 – 2015) and selected climate indices. AD: Arctic Dipole index, MAM: March, April May, JJA: June, July, August; AO: Arctic Oscillation index; SA: Siberian/Alaskan index (2004 – 2013); IER: Ice extent/retreat index (2005 – 2015). Simulations were initiated from Bering Strait and Chukotka Peninsula release locations using surface-oriented behavior. **$p$-value < 0.05 (darker shading), *0.05 ≤ $p$-value < 0.10 (lighter shading). Red (blue) represents a positive (negative) correlation.

| Bering Strait | | | | | | Kotzebue Sound | | | | | |
|---|---|---|---|---|---|---|---|---|---|---|---|
| **Latitude COG Index** | **AD (MAM)** | **AD (JJA)** | **AO** | **SA** | **IER** | **Latitude COG Index** | **AD (MAM)** | **AD (JJA)** | **AO** | **SA** | **IER** |
| All dates | -0.18 | -0.27 | 0.19 | 0.41 | -0.43 | All dates | 0.03 | 0.70* | -0.22 | -0.58* | 0.07 |
| 1-Jan | -0.23 | 0.19 | -0.13 | -0.07 | -0.43 | 1-Jan | -0.14 | 0.36 | -0.06 | -0.48 | -0.12 |
| 15-Jan | -0.08 | 0.21 | -0.08 | -0.10 | -0.19 | 15-Jan | 0.13 | 0.42 | -0.22 | -0.44 | -0.41 |
| 1-Feb | -0.17 | 0.27 | -0.14 | -0.11 | -0.05 | 1-Feb | 0.06 | -0.07 | 0.16 | -0.06 | -0.09 |
| 15-Feb | -0.30 | -0.23 | 0.19 | 0.57* | -0.28 | 15-Feb | 0.32 | 0.10 | -0.17 | -0.56* | 0.02 |
| 1-Mar | 0.00 | -0.44 | 0.22 | 0.26 | -0.55* | 1-Mar | 0.06 | 0.77** | -0.29 | -0.51 | 0.39 |
| 15-Mar | -0.01 | -0.32 | 0.51* | 0.58* | -0.24 | 15-Mar | 0.02 | 0.57* | -0.33 | -0.15 | -0.10 |
| 1-Apr | -0.31 | -0.66** | 0.44 | 0.40 | 0.00 | 1-Apr | 0.10 | 0.09 | 0.13 | 0.28 | -0.24 |
| 15-Apr | -0.11 | -0.64** | 0.02 | 0.30 | -0.53* | 15-Apr | -0.07 | -0.23 | 0.15 | 0.28 | -0.08 |
| 1-May | -0.15 | -0.38 | 0.37 | 0.87** | 0.05 | 1-May | 0.08 | -0.63** | 0.49 | 0.00 | -0.16 |
| 15-May | 0.15 | -0.33 | 0.13 | 0.32 | -0.77** | 15-May | 0.64* | -0.09 | -0.12 | -0.35 | -0.09 |
| **Longitude COG Index** | **AD (MAM)** | **AD (JJA)** | **AO** | **SA** | **IER** | **Longitude COG Index** | **AD (MAM)** | **AD (JJA)** | **AO** | **SA** | **IER** |
| All dates | 0.18 | 0.07 | 0.16 | 0.13 | 0.55* | All dates | -0.64** | -0.11 | 0.71** | 0.39 | 0.47 |
| 1-Jan | -0.07 | 0.34 | 0.55* | 0.12 | 0.41 | 1-Jan | -0.50* | -0.32 | 0.36 | 0.60* | 0.45 |
| 15-Jan | 0.20 | 0.12 | -0.19 | -0.02 | 0.42 | 15-Jan | -0.27 | -0.22 | 0.61** | 0.45 | 0.01 |
| 1-Feb | 0.53* | 0.13 | -0.04 | -0.51 | 0.13 | 1-Feb | -0.58** | -0.04 | 0.22 | -0.15 | 0.26 |
| 15-Feb | 0.41 | 0.06 | -0.01 | 0.10 | 0.31 | 15-Feb | -0.28 | 0.17 | 0.34 | 0.31 | -0.03 |
| 1-Mar | 0.18 | 0.30 | 0.07 | 0.10 | 0.72* | 1-Mar | -0.21 | -0.18 | 0.39 | 0.66** | 0.23 |
| 15-Mar | -0.25 | 0.12 | 0.12 | 0.42 | 0.72* | 15-Mar | 0.22 | -0.20 | 0.41 | 0.08 | 0.37 |
| 1-Apr | 0.03 | -0.12 | 0.14 | 0.10 | 0.50 | 1-Apr | -0.21 | 0.02 | -0.25 | -0.54 | 0.24 |
| 15-Apr | 0.02 | -0.10 | 0.50* | 0.24 | 0.50 | 15-Apr | 0.09 | 0.23 | -0.08 | -0.42 | -0.10 |
| 1-May | 0.12 | -0.12 | 0.02 | 0.36 | 0.37 | 1-May | -0.12 | 0.65** | -0.44 | -0.24 | -0.11 |
| 15-May | 0.37 | 0.01 | -0.26 | 0.02 | 0.37 | 15-May | -0.13 | 0.13 | 0.15 | 0.02 | -0.26 |

When the five climate indices were compared over the 2004 – 2015 period, no obvious trends were noted (Fig. S3), though the summer AD index was negative from 2004 – 2012 (Fig. S3 b) and the SA index was positive between 2004 – 2008 (Fig. S3 d). Correlations between the climate indices were not significant (Table S1).

## 4. Discussion

Results of our biophysical transport modeling study suggest that the source of aggregations of polar cod and saffron cod larvae and early juveniles observed in the Chukchi Sea during the 2012 and 2013 Arctic Eis surveys were most likely from the northern Bering Sea or the southern Chukchi Sea. In particular, Bering Strait and the Chukotka Peninsula were identified as potential spawning and/or hatching locations of polar cod. Our findings support other research that has suggested the existence of a number of nearshore, shallow spawning grounds in the North American and Siberian Arctic (Craig et al., 1982; Thanassekos and Fortier, 2012; Logerwell et al., 2015). In addition, our results align well with those of Ponomarenko (1968) and Sunnanå and Christiansen (1997), which suggested that polar cod spawn in the northern Bering and southern Chukchi seas. For saffron cod, simulations that produced results most similar to observed field distributions were those initiated from Bering Strait and Kotzebue Sound. Saffron cod are

742 believed to spawn demersally under ice in shallow, nearshore areas (Morrow, 1980; Fechhelm et
743 al., 1985; Wolotira, 1985; Johnson, 1995; Mecklenburg et al., 2002) and our results are supported
744 by observations of saffron cod in spawning condition in nearshore areas along the coast, such as
745 Kotzebue Sound (A. Whiting, Native Village of Kotzebue, personal communication). Strong and
746 consistent correlations between field observations and modeled distributions across several
747 behaviors and over a wide range of dates lends further support to the hypothesis that Kotzebue
748 Sound is an important spawning habitat for saffron cod. Furthermore, correlations between
749 simulated and observed saffron cod distributions were strongest from early April to mid-May.
750 These results match well with the timing of peak hatching for saffron cod, which occurs in April
751 and May, prior to the warming of coastal waters in the Arctic and northern Pacific (Wolotira,
752 1985).
753 Simulated distributions and sizes of polar cod overlapped with those estimated by the
754 Arctic Eis program's acoustic-trawl survey in 2012, yet there was poor overlap in 2013, as
755 evidenced by the lack of significant correlations with any of the release locations or dates in that
756 year. A comparison of particle locations on 1 September showed strong variability in dispersal
757 patterns between the two years, with reduced overlap of particles with the Arctic Eis survey grid
758 in 2013 (18.72%) compared to 2012 (22.05%)(Fig. S1). In 2012, simulated particles on the
759 Chukchi Shelf were concentrated along the Central Channel or the Western Pathway towards
760 Herald Canyon. Additional concentrations were found along the Alaskan coastline and formed a
761 thick band between Herald and Hanna shoals, which extended eastward towards the coast
762 between Icy Cape and Wainwright, and towards the head of Barrow Canyon (Fig. S1). High
763 concentrations of simulated larvae in this region are in agreement with other studies that have
764 noted high abundances of polar cod ELS in the northern Chukchi Sea offshore of Wainwright (De
765 Robertis et al., 2017b; Vestfals et al., 2019; Deary et al., in review). In contrast, simulated polar
766 cod in 2013 were mainly distributed outside of the Arctic Eis survey grid (Fig. S1) and found
767 mostly outside of the areas of the shelf that were occupied in 2012. There were some similarities
768 between the two years, mainly along the Alaskan coastline and in the region between Herald and
769 Hanna shoals, towards Icy Cape and Wainwright, although the band in 2013 was narrower (Fig.
770 S5 – S6). Higher concentrations of simulated larvae and early juveniles were found in the western
771 portion of the Chukchi Sea in 2013, along the Chukotka Peninsula and in Long Strait, with
772 additional particles taking a more westward route towards Herald Canyon, over the northern
773 Chukchi shelf, and across the shelf break compared to 2012. While the majority of particles
774 (81.27%) were outside of the Arctic Eis survey area in 2013, limited ichthyoplankton sampling in
775 the western and northern Chukchi Sea in 2004, 2009, and 2012 during the Russian-American

776 Long-Term Census of the Arctic (RUSALCA) program encountered high abundances of polar
777 cod larvae and early juveniles in these areas, and as far west as the East Siberian Sea (Norcross et
778 al., 2006; Vestfals et al., 2019; M. Busby, NOAA, unpublished results).
779 Simulated distributions of saffron cod from the Bering Strait release location were similar
780 to those of polar cod (Fig. S7). Given that the starting locations and behavior scenarios were
781 identical between species, the distributional differences can be attributed to the different
782 temperature-dependent growth rates used for each species in the IBMs. As fish grow, changes in
783 body length affect their swimming speed. This, in turn, affects their vertical position in the water
784 column, and ultimately, the horizontal transport of their ELS through exposure to different flow
785 schemes (Vikebø et al., 2005; Fiksen et al., 2007; Leis, 2007). Here, the slower growth rates of
786 saffron cod would result in individuals being located in the surface layer for longer in comparison
787 to polar cod. Particles from simulations initiated in Kotzebue Sound were consistently retained
788 within the Sound or were advected northward along the Alaskan coastline (Fig. S8). Age-0
789 saffron cod are known to occupy shallow, nearshore habitats (Wolotira, 1985; Logerwell et al.,
790 2015; De Robertis et al., 2017b) and have been found in high abundances from Kotzebue Sound
791 to north of Cape Lisburne in late summer (De Robertis et al., 2017b; Vestfals et al., 2019). Recent
792 surveys in the eastern Chukchi Sea in 2017 encountered high abundances of saffron cod larvae
793 around Kotzebue Sound in late spring, though by late summer they were found in nearshore areas
794 from northern Kotzebue Sound to around Cape Lisburne (Deary et al., in review). These findings,
795 combined with our modeling results, suggest that saffron cod spawned in Kotzebue Sound are
796 retained there or are transported northwards by currents to juvenile nursery habitats along the
797 coast. Over time, fish have evolved to spawn in areas where bathymetric features and prevailing
798 currents transport their larvae to or retain them within suitable nursery habitats (Iles and Sinclair,
799 1982; Bailey and Picquelle, 2002; Bailey et al., 2008; Duffy-Anderson et al., 2013). Satellite
800 tracked drifters with near-surface drogues (Danielson and Whiting, 2016) and numerical
801 modeling (Panteleev et al., 2013) show that a gyre forms in Kotzebue Sound, which was also
802 evident in the PAROMS model output. Hence, the circulation in and around Kotzebue Sound may
803 be especially conducive to larval retention and/or delivery to juvenile nursery habitats. The
804 retentive nature of Kotzebue Sound is also supported by the results of our analyses, which
805 showed COGs that were consistently located in northern Kotzebue Sound (Fig. 5 b), along with
806 low inertia over the time series (Fig. 6 d).
807 The strong year-to-year variability in simulated distributions of polar cod and saffron cod
808 suggests that transport of their early life stages is highly sensitive to variations in flow across the
809 Chukchi shelf. Only simulations from Kotzebue Sound showed relatively consistent dispersal

patterns between years. Observed differences in simulated particle distributions across the broader Chukchi Shelf in 2012 and 2013 can be linked to differences in oceanographic and atmospheric conditions between the two years. In 2013, persistent northeasterly winds in late summer led to flow reversals over much of the northeast Chukchi Sea, which limited the northward extent of the ACC and advected Arctic waters onto the Chukchi Shelf via Barrow Canyon (Danielson et al., 2017). This is consistent with simulated particles following a more westward pathway along the shelf in 2013, compared to 2012 (Fig. S1). The inflow of Pacific waters through Bering Strait is bathymetrically steered along either Herald Canyon, the Central Channel, or along the Alaskan coast; however, this inflow can be driven towards the western portion of the shelf during periods with easterly winds (Windsor and Chapman, 2004). Similarly, Bond et al. (2018) described a stronger than normal flow pattern through Bering Strait, where a disproportionate portion of the flow travels northwest toward and beyond Wrangel Island rather than joining the ACC, which they linked to anomalous winds from the east-northeast. Indeed, winds were more persistent from the northeast and annual transport through Bering Strait was higher in 2013 (~ 1.1 Sv) compared to 2012 (~ 0.7 Sv) (Woodgate et al., 2015).

One curious aspect of the modeled larval aggregations was that they appeared to aggregate in long banded arrangements stretching from the Barrow Canyon region in the NE Chukchi Sea across the shelf toward the west. Examination of the model hydrographic fields in 2012 (Fig. S9) revealed that the larvae were accumulating in the vicinity of the ice-edge frontal zone (Fig. S9 a), which is delineated by a change of density (salinity (Fig. S9 e) and temperature (Fig. S9 c)) from the open water zone south of the marginal ice zone to under the pack ice. Recent investigations into the hydrographic structure associated with ice edge fronts and the melting of ice on the Chukchi shelf has revealed convergent zones associated with the ice and thermohaline fields (Lu et al., 2020a; 2020b). These frontal zones can extend several meters (up to 15 m) below the surface and likely provide enhanced feeding opportunities for surface-oriented larvae and early juveniles by maintaining them in close proximity to the ice edge, where they can take advantage of copepod production fueled by ice-edge phytoplankton blooms (Søreide et al., 2010; Perrette et al., 2011), as well as the higher concentrations of food particles that tend to accumulate in convergent frontal zones (Bakun, 2006). For surface-oriented larvae, these frontal zones may act as a barrier to northward advection, however, this may not be the case for species that live at or migrate to depths below the vertical extent of the frontal zone. Much work remains to be done to determine to what extent polar cod larvae in the field are actually subject to the influences of the convergent ice-edge fronts, but the combination of our work and the ice edge modeling study

raises many interesting questions, provides new testable hypotheses, and provides new ways to think about the early life stages of polar cod and other Arctic species.

Correlations between location indices derived from the simulation output and several climate indices provide evidence that dispersal of polar cod and saffron cod ELS are likely sensitive to environmental forcing. During periods that were characterized by colder conditions in the Pacific Arctic (i.e., a positive AO index, with a strong jet stream that retains cold air over the polar region (Thompson and Wallace, 2000); a negative AD index, where more sea-ice remains in the western Arctic (Watanabe et al., 2006; Wu et al., 2006); a positive SA index, with anomalously strong northwesterly winds and heavy ice cover (Fang and Wallace 1994; Overland et al., 2002); and a greater ice extent and later ice retreat (Okkonen et al., 2019)), cod ELS were found farther south and east compared to periods that represented warmer conditions in the region. The findings of our study have important implications for polar cod and saffron cod connectivity between the Chukchi and Beaufort seas. Our results suggest that in warmer years with greater Pacific inflow and an earlier sea-ice retreat (e.g., 2005, 2010, and 2011 in Figs. S5 – S8), a higher proportion of larvae spawned in the northern Bering or southern Chukchi seas would be transported northwestward towards Herald Canyon and across the northern Chukchi shelf (see Okkonen et al., 2019, their Fig. 6B), which would result in a greater contribution to populations in the northern Chukchi and western Beaufort seas. In contrast, during colder years with reduced Pacific inflow and a later ice retreat (e.g., 2006, 2009, and 2012 in Figs. S5 – S8), larvae would be advected along the ice edge towards the Alaskan coast, with a greater proportion of the population retained in the eastern Chukchi Sea (see Okkonen et al., 2019, their Fig. 6A). The timing and pattern of sea-ice retreat across the Chukchi shelf has been linked to the strength of the Pacific-Arctic pressure head, which is influenced by the strength and location of the Beaufort Sea High pressure cell and its associated winds (Danielson et al., 2014; Okkonen et al., 2019). A stronger Pacific-Arctic pressure head (i.e., 2005, 2007, 2009, 2011, and 2015) was associated with greater northward volume and property fluxes along the Alaskan coast (i.e. a stronger Alaska Coastal Current), which promoted earlier ice retreat across the eastern Chukchi shelf (Okkonen et al., 2019). In contrast, a weaker pressure head (i.e., 2006, 2008, 2010, 2012 – 2014) was associated with lower volume and property fluxes along the Alaskan coast and slower, less directionally-biased ice retreat across the Chukchi shelf (Okkonen et al., 2019). Similarly, Luchin and Panteleev (2014) found that during warm years, the inflow of Pacific water through Bering Strait spread widely along the Siberian coast, with extensive transport through Herald Channel. In cold years, however, the inflow of warm Pacific water was reduced and mostly flowed along the Alaskan coast before exiting the shelf through Barrow Canyon. Thus, as

877 continued Arctic warming further impacts sea-ice extent and timing of sea ice retreat in the
878 Chukchi Sea, we anticipate that polar cod and saffron cod ELS will be affected by concomitant
879 changes in flow across the shelf, which will likely affect population connectivity between the
880 northern Bering, Chukchi and Beaufort seas.
881 Simulations that produced saffron cod distributions most similar to Arctic Eis field
882 observations were those initiated from Bering Strait and Kotzebue Sound, particularly those with
883 a passive component. This result was not surprising, as saffron cod larvae grow slowly at low
884 temperatures and as such, their dispersal is more likely to be affected by currents than by their
885 behavior. However, larvae are not passive particles that drift along with currents and even first-
886 feeding larvae have the ability to control temperature, salinity, light, turbulence and food
887 concentrations by migrating vertically, which in turn contributes to their horizontal movement
888 (Norcross and Shaw, 1984; Boehlert and Mundy, 1988; Hare and Govoni, 2005; Hurst et al.,
889 2009). Late-stage larvae and pelagic juveniles have also been shown to have considerable control
890 over their speed, direction, and position in the water column (Olla et al., 1996; Leis and Carson-
891 Ewart, 1997, 1999). Even slight differences in behavior can have long-term and large-scale
892 consequences, since vertical positioning influences the drift trajectory of the larva, and thereby
893 the physical environment it experiences along the way (Vikebø et al., 2007). Our simulation
894 results showed that behavior did indeed have a strong effect on larval dispersal (Fig. S4, Tables 3
895 and 4). While detailed information about the vertical distribution of saffron cod larvae is not
896 currently available, newly hatched larvae spend between 2–3 months as plankton before
897 descending to the bottom in mid-summer, between 39 and 56 mm in length in the Pacific and 55
898 and 60 mm in the Arctic (Wolotira, 1985); larger age-0 fish can still be found in surface waters in
899 late summer (Eisner et al., 2012). Similarly, polar cod larvae have been shown to be surface-
900 oriented in the first few months of life (Spencer et al., 2020; B. Laurel, unpublished results),
901 moving deeper as they develop (Borkin et al., 1986), with pelagic juveniles descending deeper in
902 the water column in late summer, between 30 and 55 mm in length (Matarese et al., 1989;
903 Ponomarenko, 2000; Bouchard and Fortier, 2011). Recent repeat acoustic surveys in the eastern
904 Chukchi Sea from mid- to late-summer in 2019 indicated that age-0 polar cod moved deeper in
905 the water column and underwent DVM as the season progressed (Levine et al., 2020). While
906 these data were not available at the time of our study, this behavior was considered in our
907 preliminary simulations, as previous research has shown that polar cod undergo DVM in other
908 areas of the Arctic (Borkin et al., 1986; Bouchard et al., 2016). However, the sizes at which fish
909 begin their DVM and the depths to which they migrate had to be estimated for the Chukchi Sea,
910 which is shallower (< 40 m) than the other regions where DVM behavior has been observed. We

911 ultimately chose the surface-oriented behavior to model growth and dispersal from 2004 – 2005,
912 as this behavior was most strongly correlated with observed distributions in the field, though the
913 overall results and conclusions were similar when based on the more complex surface-oriented
914 behavior for early larval stages that moved deeper with ontogeny (C. Vestfals, unpublished
915 results). The new information provided by the repeat acoustic surveys on the depth distribution of
916 polar cod ELS, the sizes at which they begin to vertically migrate, and the depths to which they
917 migrate (Levine et al., 2020) will be invaluable to future modeling efforts in the Chukchi Sea.
918 While climate-driven changes in advective transport and mixing will affect the dispersal
919 and ultimately the distribution of larvae, the temperatures they experience during the drift period
920 will, in turn affect their growth rates and their survival (Vikebø et al., 2005, 2007). We found
921 differences in simulated lengths on 1 September between release locations, hatch dates, and
922 species. The greater lengths attained by larvae hatching in southern locations can be attributed to
923 warmer temperatures in the Bering Sea, in general, which results in faster growth of larvae
924 hatching there compared to the Chukchi Sea. In spring, solar heating and the inflow of warmer
925 water from the Bering Sea leads to rapid warming in the Chukchi Sea. Thus, the temperature
926 conditions experienced by larvae hatching at later dates are more similar between regions
927 compared to those hatching during the winter months. While polar cod simulated lengths aligned
928 fairly well with fish ≤ 45 mm in length observed in the Arctic Eis acoustic-trawl survey, those for
929 saffron cod did not, with much smaller simulated sizes than field estimates. The differences in
930 simulated sizes between species result from assuming higher growth rates at lower temperatures
931 for polar cod compared to saffron cod based on laboratory studies (Laurel et al., 2016; B. Laurel,
932 unpublished results). The difference between observed and simulated lengths for saffron cod
933 could have resulted from incorrectly specified growth in the IBM, incorrect temperatures in the
934 model, strong size-selective mortality, incorrect assumptions about hatch dates, or other factors. It
935 should be emphasized that the final estimates of acoustic-trawl survey abundance at length were
936 sensitive to the selectivity parameters used in the calculations, particularly for the smallest size
937 classes, which are poorly retained by the trawls (De Robertis et al., 2017a, b). In particular, 2012
938 abundance estimates for fish < 25 mm in length were effectively zero for both species across the
939 entire survey region, which was most certainly due to the ineffectiveness of the Cantrawl gear at
940 catching these smaller-sized fish, rather than a lack of presence of these sizes over the eastern
941 Chukchi shelf. While use of the modified Marinovich trawl in 2013 improved the abundance
942 estimates of fish in the 15 – 25 mm range, estimated abundances of fish < 15 mm remained at
943 zero across the entire survey region, which clearly does not reflect their true abundance and
944 distribution. Recent studies of polar cod and saffron cod ELS in the Chukchi Sea have found the

945 presence of larvae < 25 mm in length in the Arctic Eis survey area during late summer (Vestfals
946 et al., 2019; Deary et al., in review). In other regions of the Arctic, polar cod lengths in late
947 summer can vary in size from 10 mm for fish hatched late in July, to 50 mm for young-of-the-
948 year fish hatched early in January (Bouchard and Fortier, 2011). Thus, our simulation results for
949 polar cod from the northern hatching locations (Bering Strait, Chukotka Peninsula, Kotzebue
950 Sound) and saffron cod, in general, may reflect sizes in the field not captured in the acoustic-trawl
951 survey estimates. However, our models clearly underestimated growth in both species. Field-
952 based estimates of polar cod growth range from 0.27 – 0.51 mm $day^{-1}$ (Bouchard and Fortier,
953 2011; Vestfals et al., 2019; Deary et al., in review), which are higher than the laboratory estimates
954 used in this study (0.04 – 0.46 mm $day^{-1}$, Koenker et al., 2018; Laurel et al., 2017), particularly
955 for smaller polar cod larvae and those growing at lower temperatures (Fig. 2). As only the
956 survivors of size-based predation are encountered in field samples, which selects for faster
957 growing individuals (Bailey and Houde, 1989; Litvak and Leggett, 1992), field-based growth
958 estimates are often higher than those derived in the laboratory because fish larvae are known to
959 grow and survive better on natural prey (Sargent et al., 1999; Evjemo et al., 2003).
960 The laboratory-derived growth rates used in our model likely underestimated saffron cod
961 growth in the field, which contributed to the smaller simulated lengths compared to the lengths
962 estimated by the Arctic Eis acoustic-trawl surveys. Unfortunately, a growth equation for larger
963 stages of saffron cod is not currently available and we used growth of a related gadid, walleye
964 pollock, to model growth in the IBM. While walleye pollock ELS exhibit linear growth similar to
965 that of saffron cod (Porter and Bailey, 2007; B. Laurel, NOAA, personal communication), some
966 component of saffron growth was not fully captured in our model. Saffron cod may have a
967 specific size or thermal range at which growth increases exponentially, or a particular habitat
968 factor may influence their growth. Growth of saffron cod might be slow and constant during early
969 development, but this could be followed by a period of rapid acceleration in growth. For example,
970 Pacific hake (*Merluccius productus*), another North Pacific gadiform with a similar trophic role to
971 saffron cod, grow slowly in the first 3 months of life (< 30 mm SL), after which their growth
972 accelerates (Bailey, 1982; Bailey et al., 1982; Woodbury et al., 1995). Saffron cod may also
973 experience faster growth in nearshore regions, with under-ice river plumes in coastal areas
974 providing a thermal refuge for developing eggs and larvae during winter and early spring via
975 relatively warmer freshwater runoff (Bouchard and Fortier, 2011). The solar-heated waters in
976 Kotzebue Sound, Norton Sound, and coastal areas to the south provide a major source of the heat
977 to the Alaska Coastal Current (Coachman et al., 1975; Ahlnäs and Garrison, 1984) and may also
978 provide a thermal habitat conducive for optimal growth in saffron cod. Indeed, temperatures in

Kotzebue Sound in July can exceed 12°C (Ahlnäs and Garrison, 1984), which exceeds thermal optima for some gadids, but is near the temperature of maximum growth for age-0 saffron cod ($T_{max}$ = 14.8°C) found in the lab (Laurel et al., 2016).

There are some limitations to using observations from the 2012 and 2013 Arctic Eis acoustic-trawl survey to validate our simulation results. The acoustic-trawl surveys were limited in their spatial extent and did not cover the inshore region or more northern areas of the Chukchi and Beaufort seas, or the Arctic Basin. Polar cod and saffron cod larvae may be present in these locations, so without further sampling, it is important not to rule out the northern locations as potential spawning or hatching areas. Results from the initial passive particle simulations showed that polar cod larvae hatching from more northern locations (Cape Lisburne, Hanna Shoal, and Barrow Canyon) were transported into nearshore regions in the northern Chukchi and Beaufort seas, as well as into the Arctic Basin. Due to the lack of overlap between simulated larval distributions and the Arctic Eis survey grids, which prevented model validation with field observations, further simulations from these hatching locations were not explored. However, these northern spawning/hatching locations in the Chukchi Sea may be a source of larvae for the Beaufort Sea and Arctic Basin. Indeed, small polar cod and saffron cod larvae corresponding to the sizes observed in our preliminary simulations from northern hatch locations (see Fig. S2) were collected in August 2008 around Barrow Canyon (Logerwell et al., 2015) and in 2017, small polar cod larvae were collected beyond the Chukchi shelf break in late summer/early fall (M. Busby, NOAA, personal communication.). High abundances of age-0 polar cod may also be present in the western portion of the Chukchi Sea outside the Arctic Eis survey area, as suggested by our simulations. This is consistent with large aggregations of age-0 polar cod along the western edge of the survey area in 2017, and to a lesser extent in 2019 (A. De Robertis, NOAA, R. Levine, UW, personal communication).

The PAROMS model used to drive the polar cod and saffron cod IBMs has been shown to resolve important oceanographic processes [e.g. mean flows and flow variances, wind-driven currents, continental shelf waves, seasonality of ice, and annual volume, heat, freshwater, and ice transport (Curchitser et al., 2013, 2018; Danielson et al., 2016; Danielson et al., 2020) and biological covariates (Rand et al., 2018; Lovvorn et al., 2020). Although PAROMS has relatively fine resolution (e.g. front-resolving and eddy-permitting) for basin-scale models covering a region as broad as the whole Arctic, it undoubtedly fails to accurately reproduce some submesoscale dynamics that could be important in the transport of polar cod and saffron cod larvae to nursery areas. Nonetheless, we believe that our polar cod and saffron cod IBMs can improve our understanding about the growth, transport, and connectivity of these species in the

Pacific Arctic and provides an important framework for examining transport in other key arctic species.

## 5. Conclusions

We developed the first individual-based, biophysical transport models for polar cod and saffron cod in the Pacific Arctic, which we used to reproduce observed late summer distributions of their ELS in the Chukchi Sea. The results of this study provide important information about these key forage fishes. In particular, we have identified potential spawning locations and nursery habitats for larvae and early juveniles, and have shown how the growth and dispersal of their ELS change in response to variable climate forcing. The source of observed aggregations of polar cod on the Chukchi shelf appear to be from the northern Bering and southern Chukchi seas, while spawning locations in the northern Chukchi Sea may be a source population for the western Beaufort Sea. Kotzebue Sound appears to be both an important spawning and nursery area for saffron cod, as well as a source of larvae and juveniles to nearshore nursery areas. We found strong variability in dispersal patterns among years, which were linked to changes in oceanographic and atmospheric forcing. Observed variability in the dispersal of polar cod and saffron cod ELS is likely related to changes in the strength of the Pacific-Arctic pressure head, which influences the inflow of Pacific waters into the Chukchi Sea and the timing and pattern of sea ice retreat. Understanding how connectivity between the Chukchi and Beaufort seas may change in response to Arctic warming is important if we are to understand the stock structure and population dynamics of polar cod and saffron cod in the region. Such information is essential to spatial management of Alaska's Arctic marine ecosystems.

## Declaration of Competing Interest

The authors declare that they have no known competing financial interests or personal relationships that could have appeared to influence the work reported in this paper.

## Acknowledgements

This study was supported by a grant from the North Pacific Research Board (NPRB; Project #1508) and was also funded in part by the Bureau of Ocean and Energy Management (BOEM) Award #M12AC00009 and in part with qualified outer continental shelf oil and gas revenues by the Coastal Impact Assistance Program, U.S. Fish and Wildlife Service, U.S. Department of the Interior (Contract #s: 10-CIAP-010; F12AF00188). This paper is EcoFOCI Contribution

No. EcoFOCI-N950. The authors wish to thank the scientists and volunteers that collected data on the Arctic Eis acoustic-trawl surveys, Elizabeth Drenkard, and Joakim Kjellsson for their initial assistance with TRACMASS, Alicia Billings for assistance with data processing, and Alison Deary, Esther Goldstein, and two independent reviewers for their helpful comments on this manuscript. The findings and conclusions in this paper are those of the authors and do not necessarily represent the views of the National Marine Fisheries Service. Reference to trade names does not imply endorsement by the National Marine Fisheries Service, NOAA or any of its subagencies. SLD acknowledges support from NPRB grants A91-99a and A91-00a. This manuscript is a product of the North Pacific Research Board Arctic Integrated Ecosystem Research Program, NPRB publication number ArcticIERP-XX.

**Author contributions**

**Cathleen Vestfals:** Methodology, Software, Investigation, Formal Analysis, Data Curation, Writing – Original draft preparation. **Franz Mueter:** Conceptualization, Methodology, Supervision, Writing – Reviewing and Editing. **Katherine Hedstrom:** Methodology, Data curation, Software. **Benjamin Laurel:** Methodology, Investigation, Writing – Reviewing and Editing. **Colleen Petrik:** Methodology, Software, Writing – Reviewing and Editing. **Janet Duffy-Anderson:** Conceptualization, Methodology. **Seth Danielson:** Methodology, Data curation, Writing – Reviewing and Editing.

## References


Aagaard, K., Weingartner, T.J., Danielson, S.L., Woodgate, R.A., Johnson, G.C., Whitledge, T.E., 2006. Some controls on flow and salinity in Bering Strait. Geophysical Research Letters 33, L19602.

Ahlnäs, K., Garrison, G.R., 1984. Satellite and oceanographic observations of the warm coastal current in the Chukchi Sea. Arctic 37 (3), 244-254.

Bailey, K.M., 1981. Larval transport and recruitment of Pacific hake *Merluccius productus.* Marine Ecology Progress Series 6 (1), 1-9.

Bailey, K.M., 1982. The early life history of the Pacific hake *Merluccius productus*. Fishery Bulletin 80 (3), 589-598.

Bailey, K.M., Abookire, A.A., Duffy-Anderson, J.T., 2008. Ocean transport paths for the early life history stages of offshore spawning flatfishes: a case study in the Gulf of Alaska. Fish and Fisheries 9 (1), 44-66.

Bailey, K.M., Francis, R.C., Stevens, P.R., 1982. The life history and fishery of Pacific whiting, *Merluccius productus*. NWAFC Processed Report 82-03. Northwest and Alaska Fisheries Center, National Marine Fisheries Service, U.S. Department of Commerce.

Bailey, K.M., Houde, E.D., 1989. Predation on eggs and larvae of marine fishes and the recruitment problem. In: Advances in Marine Biology. Blaxter, J., Douglas, B. (Eds.), Academic Press, Cambridge, MA, Volume 25, pp. 1-83.

Bailey, K.M., Picquelle, S.J., 2002. Larval distribution of offshore spawning flatfish in the Gulf of Alaska: potential transport pathways and enhanced onshore transport during ENSO events. Marine Ecology Progress Series 236, 205-217.

Bakun, A., 2006. Fronts and eddies as key structures in the habitat of marine fish larvae: opportunity, adaptive response and competitive advantage. Scientia Marina 70 (S2), 105-122.

Batchelder, H. P., 2006. Forward-in-time-/backward-in-time-trajectory (FITT/BITT) modeling of particles and organisms in the coastal ocean. Journal of Atmospheric and Oceanic Technology, 23 (5), 727-741.

Bauer, R.K., Stepputtis, D., Gräwe, U., Zimmermann, C., Hammer, C., 2013. Wind-induced variability in coastal larval retention areas: a case study on Western Baltic spring-spawning herring. Fisheries Oceanography, 22 (5), 388-399.

Berg L.S., 1949. Ryby presnykh vod SSSR i sopredel'nykh stran (Freshwater Fishes of the USSR and Adjacent Countries). Zoological Institute of the Academy of Sciences of the USSR, USSR, Leningrad (in Russian).

Berglund, M., Jacobi, M.N., Jonsson, P.R., 2012. Optimal selection of marine protected areas based on connectivity and habitat quality. Ecological Modelling 240, 105-112.

Björnsson, B., 1993. Swimming speed and swimming metabolism of Atlantic cod (*Gadus morhua*) in relation to available food: a laboratory study. Canadian Journal of Fisheries and Aquatic Sciences 50 (12), 2542-2551.

Boehlert, G.W., Mundy, B.C., 1988. Roles of behavioral and physical factors in larval and juvenile fish recruitment to estuarine nursery areas. In: American Fisheries Society Symposium, Weinstein, M.P. (Ed.), American Fisheries Society, Bethesda, MD, Volume 3 (5), pp. 1-67.

Bond, N., Stabeno, P., Napp, J., 2018. Flow patterns in the Chukchi Sea based on an ocean reanalysis, June through October 1979–2014. Deep Sea Research Part II 152, 35-47.

Borkin, L.V., Ozhigin V.K., Shleinik V.N., 1986. Effect of oceanographical factors on the abundance of the Barents Sea polar cod year classes. In: The effect of oceanographic conditions on distribution and population dynamics of commercial fish stocks in the Barents Sea, vol. 169.

Bouchard, C., Fortier, L., 2008. Effects of polynyas on the hatching season, early growth and survival of polar cod *Boreogadus saida* in the Laptev Sea. Marine Ecology Progress Series 355, 247-256.

Bouchard, C., Fortier, L., 2011. Circum-arctic comparison of the hatching season of polar cod *Boreogadus saida*: a test of the freshwater winter refuge hypothesis. Progress in Oceanography 9, 105-116.

Bouchard, C., Mollard, S., Suzuki, K., Robert, D., Fortier, L., 2016. Contrasting the early life histories of sympatric Arctic gadids *Boreogadus saida* and *Arctogadus glacialis* in the Canadian Beaufort Sea. Polar Biology 39, 1005-1022.

Budgell, W.P., 2005. Numerical simulation of ice-ocean variability in the Barents Sea region. Ocean Dynamics 55 (3-4), 370-387.

Calò, A., Lett, C., Mourre, B., Pérez-Ruzafa, Á., García-Charton, J.A., 2018. Use of Lagrangian simulations to hindcast the geographical position of propagule release zones in a Mediterranean coastal fish. Marine environmental research, 134, 16-27.

Carton, J.A., Giese, B.S., 2008. A Reanalysis of Ocean Climate Using Simple Ocean Data Assimilation (SODA). Monthly Weather Review 136, 2999-3017. https://doi.org/10.1175/2007MWR1978.1.

Chassignet, E.P., Hurlburt, H.E., Metzger, E.J., Smedstad, O.M., Cummings, J., Halliwell, G.R., Bleck, R., Baraille, R., Wallcraft, A.J., Lozano, C. et al., 2009. U.S. GODAE: Global Ocean Prediction with the HYbrid Coordinate Ocean Model (HYCOM). Oceanography 22 (2), 64-75.

Chen, A., Yoshida, H., Sakurai, Y., 2008. Reproductive behavior of Saffron cod in captivity. Scientific Reports of Hokkaido Fisheries Experimental Station 73, 35-44.

Christensen, A., Daewel, U., Jensen, H., Mosegaard, H., John, M. S., Schrum, C., 2007. Hydrodynamic backtracking of fish larvae by individual-based modelling. Marine Ecology Progress Series, 347, 221-232.

Coachman, L.K., Aagaard, K., Tripp, R.B., 1975. Bering Strait: the regional physical oceanography. University of Washington Press, Seattle.

Coachman, L.K., Aagaard, K., 1981. Re-evaluation of water transports in the vicinity of Bering Strait, The Eastern Bering Sea Shelf: Oceanography and Resources. Hood, D.W., Calder, J.A. (Eds.), National Oceanic and Atmospheric Administration, Washington, D.C., Volume 1, pp. 95–110.

Comiso, J.C., Parkinson, C.L., Gersten, R., Stock, L., 2008. Accelerated decline in the Arctic sea ice cover. Geophysical Research Letters 35, L01703.

Corlett, W.B., Pickart, R.S., 2017. The Chukchi slope current. Progress in Oceanography 153, 50-65.

Craig, P.C., Griffiths, W.B., Haldorson, L., McElderry, H., 1982. Ecological studies of Arctic Cod (*Boreogadus saida*) in Beaufort Sea coastal waters. Canadian Journal of Fisheries and Aquatic Sciences 39, 395-406

Curchitser, E.N., Hedstrom, K., Danielson, S., Weingartner, T., 2013. Adaptation of an Arctic Circulation Model. U.S. Dept. of the Interior, Bureau of Ocean Energy Management, Headquarters, Herndon, VA. OCS Study BOEM, M10PC00116.

Curchitser, E.N., K. Hedstrom, S. Danielson, Kasper, J., 2017. Development of a Very High-Resolution Regional Circulation Model of Beaufort Sea Nearshore Areas. U.S. Dept. of the Interior, Bureau of Ocean Energy Management, Alaska OCS Region, Anchorage, AK. OCS Study BOEM 2018-018. 81 pp.

Dai, A., Qian, T., Trenberth, K.E., Milliman, J.D., 2009. Changes in continental freshwater discharge from 1948 to 2004. Journal of Climate 22 (10), 2773-2792.

Danielson, S.L., Weingartner, T.J., Hedstrom, K.S., Aagaard, K., Woodgate, R., Curchitser, E., Stabeno, P.J., 2014. Coupled wind-forced controls of the Bering-Chukchi shelf circulation and the Bering Strait throughflow: Ekman transport, continental shelf waves, and variations of the Pacific–Arctic sea surface height gradient. Progress in Oceanography 125, 40-61. https://doi.org/10.1016/j. pocean.2014.04.006.

Danielson, S.L., Hedstrom, K.S., Weingartner, T.J., 2016. Bering-Chukchi circulation pathways, North Pacific Research Board 2016 Final Report, NPRB project #1308, University of Alaska Fairbanks, Fairbanks, AK.

Danielson, S.L., Whiting, A. 2016. 2015 Circulation and Hydrographic Structure of Kotzebue Sound. Final Report. Northwest Arctic Borough Science Steering Committee. Native Village of Kotzebue, Kotzebue, AK.

Danielson, S.L., Eisner, L., Ladd, C., Mordy, C., Sousa, L., Weingartner, T.J., 2017. A comparison between late summer 2012 and 2013 water masses, macronutrients, and phytoplankton standing crops in the northern Bering and Chukchi Seas. Deep Sea Research Part II 135, 7-26.

Danielson, S.L., Ahkinga, O., Ashjian, C., Basyuk, E., Cooper, L.W., Eisner, L., Farley, E., Iken, K.B., Grebmeier, J.M., Juranek, L., Khen, G., Jayne, S., Kikuchi, T., Ladd, C, Lu, K.,

McCabe, R., Moore, GWK, Nishino, S., Okkonen, S.R., Ozenna, F., Pickart, R.S., Polyakov, I., Stabeno, P.J., Wood, K., Williams, W.J., Woodgate, R.A., Weingartner, T.J., 2020a. Manifestation and consequences of warming and altered heat fluxes over the Bering and Chukchi Sea continental shelves. Deep Sea Research Part II 177,,104781.

Danielson, S.L., Hennon, T.D., Hedstrom, K.S., Pnyushkov, A.V., Polyakov, I.V., Carmack, E., Filchuk, K., Janout, M., Makhotin, M., Williams, W.J., Padman, L., 2020b. Oceanic routing of wind-sourced energy along the Arctic continental shelves. Frontiers in Marine Science, 7, 509.

Deary, A.L., Vestfals, C.D., Logerwell, E.A., Goldstein, E.D., Stabeno, P.J., Danielson, S.L., Mueter, F.J., Duffy-Anderson, J.T., In Review. Seasonal abundance, distribution, and growth of the early life stages of Polar Cod (*Boreogadus saida*) and Saffron Cod (*Eleginus gracilis*) in the US Arctic during a warm year. Polar Biology.

De Robertis, A., Taylor, K., Williams, K., Wilson, C.D. 2017a. Species and size selectivity of two midwater trawls used in an acoustic survey of the Alaska Arctic. Deep Sea Research Part II 135, 40-50.

De Robertis A., Taylor, K., Wilson, C., Farley, E. 2017b. Abundance and distribution of Arctic cod (*Boreogadus saida*) and other pelagic fishes over the US Continental Shelf of the Northern Bering and Chukchi Seas. Deep Sea Research Part II 135, 51-65.

Döös, K., 1995. Inter-ocean exchange of water masses. Journal of Geophysical Research 100, 13499-13514.

Döös, K., Engqvist, A., 2007. Assessment of water exchange between a discharge region and the open sea – a comparison of different methodological concepts. Estuarine and Coastal Shelf Science 74, 585-597.

Drijfhout, S., de Vries, P., Döös, K., Coward, A., 2003. Impact of eddy-induced transport of the Lagrangian structure of the upper branch of the thermohaline circulation. Journal of Physical Oceanography 33, 2141-2155.

Duffy-Anderson, J.T., Blood, D.M., Cheng, W., Ciannelli, L., Matarese, A.C., Sohn, D., Vance, T.C., Vestfals, C., 2013. Combining field observations and modeling approaches to examine Greenland halibut (*Reinhardtius hippoglossoides*) early life ecology in the southeastern Bering Sea. Journal of Sea Research 75, 96-109.

Egbert, G.D., Erofeeva, S.Y., 2002. Efficient inverse modeling of barotropic ocean tides. Journal of Atmospheric and Oceanic Technology 19 (2), 183-204.

Eisner, L., Hillgruber, N., Martinson, E., Maselko, J., 2012. Pelagic fish and zooplankton species assemblages in relation to water mass characteristics in the northern Bering and southeast Chukchi seas. Polar Biology 36, 87-113.

https://epsg.io/3572, accessed 16 September, 2019.

ESRI, 2017. ArcGIS desktop: release 10.4. Environmental Systems Research Institute, Redlands, CA.

Evjemo, J.O., Reitan, K.I., Olsen, Y., 2003. Copepods as live food organisms in the larval rearing of halibut larvae (*Hippoglossus hippoglossus* L.) with special emphasis on the nutritional value. Aquaculture 227 (1-4), 191-210.

Fang, Z., Wallace, J.M., 1994. Arctic sea ice variability on a timescale of weeks and its relation to atmospheric forcing. Journal of Climate 7 (12), 1897-1914.

Fechhelm, R.G., Craig, P.C., Baker, J.S., Gallaway, B.J., 1985. Fish distribution and use of nearshore waters in the northeastern Chukchi Sea. In: US Department of Commerce, NOAA, and US Department of the Interior, Minerals Management Service, Outer Continental Shelf Environmental Assessment Program final report. Volume 32, pp. 121-298.

Fiksen, Ø., Jørgensen, C., Kristiansen, T., Vikebø, F., Huse, G. 2007. Linking behavioural ecology and oceanography: larval behaviour determines growth, mortality and dispersal. Marine Ecology Progress Series 347, 195-205.

Gibson, G.A., Stockhausen, W.T., Coyle, K.O., Hinckley, S., Parada, C., Hermann, A.J., Doyle, M., Ladd, C., 2019. An individual-based model for sablefish: Exploring the connectivity between potential spawning and nursery grounds in the Gulf of Alaska. Deep Sea Research Part II 165, 89-112.

Govoni, J.J., 2005. Fisheries oceanography and the ecology of early life histories of fishes: a perspective over fifty years. Scientia marina 69 (S1), 125-137.

Grebmeier, J.M., McRoy, C.P., Feder, H.M., 1988. Pelagic-benthic coupling on the shelf of the northern Bering and Chukchi seas.Food-supplysourceand benthic biomass. Marine Ecology Progress Series 48, 57-67. https://doi.org/10.3354/ meps048057.

Hauri, C., Danielson, S., McDonnell, A.M., Hopcroft, R.R., Winsor, P., Shipton, P., Lalande, C., Stafford, K.M., Horne, J.K., Cooper, L.W., Grebmeier, J.M., 2018. From sea ice to seals: a moored marine ecosystem observatory in the Arctic. Ocean Science 14 (6), 1423-1433.

Hare, J.A., Govoni, J.J., 2005. Comparison of average larval fish vertical distributions among species exhibiting different transport pathways on the southeast United States continental shelf. Fishery Bulletin 103 (4), 728-736.

Hinckley, S., Hermann, A.J., Megrey, B.A., 1996. Development of a spatially explicit, individual-based model of marine fish early life history. Marine Ecology Progress Series 139, 47-68.

Hollowed, A.B., Bailey, K.M., 1989. New perspectives on the relationship between recruitment of Pacific hake (*Merluccius productus*) and the ocean environment. In: Effects of Ocean Variability on Recruitment and an Evaluation of Parameters Used in Stock Assessment Models. Beamish, R.J., McFarlane, G.A. (Eds.), Canadian Special Publication of Fisheries and Aquatic Sciences 108, 207-220.

Hurst, T.P., Cooper, D.W., Scheingross, J.S., Seale, E.M., Laurel, B.J., Spencer, M.L., 2009. Effects of ontogeny, temperature, and light on vertical movements of larval Pacific cod (*Gadus macrocephalus*). Fisheries Oceanography 18 (5), 301-311.

ICES CM, 1988. Preliminary report of the international 0-group fish survey in the Barents Sea and adjacent waters in August-September 1988. In: ICES Council Meeting

Iles, T.D., Sinclair M., 1982. Atlantic herring: stock discreteness and abundance. Science 215, 627-633.

Jacobi, M.N., Jonsson, P.R., 2011. Optimal networks of nature reserves can be found through eigenvalue perturbation theory of the connectivity matrix. Ecological Applications 21 (5), 1861-1870.

Johnson, J.J., 1995. Description and comparison of two populations of Saffron Cod (*Eleginus gracilis*) from Western Canadian Arctic Coastal Waters. Master's Thesis, University of Manitoba, Canada, unpublished.

Koenker, B., Laurel, B.J., Copeman, L.A., Ciannelli, L., 2018. Effects of temperature and food availability on the survival and growth of larval Arctic cod (*Boreogadus saida*) and walleye pollock (*Gadus chalcogrammus*). ICES Journal of Marine Science 75, 2386-2402.

Kwok, R., Cunningham, G.F., Wensnahan, M., Rigor, I., Zwally, H.J., Yi, D., 2009. Thinning and volume loss of the Arctic Ocean sea ice cover: 2003–2008. Journal of Geophysical Research: Oceans (1978–2012), 114 (C7).

Lafrance, P., 2009. Saison d'éclosion et survie des stades larvaires et juvéniles chez la morue arctique (*Boreogadus saida*) du sud-est de la mer de Beaufort. Ph.D. thesis. Université Laval, Canada, unpublished (in French, with English Abstract).

Laurel, B.J., Spencer, M., Iseri, P., Copeman, L.A., 2016. Temperature-dependent growth and behavior of juvenile Arctic cod (*Boreogadus saida*) and co-occurring North Pacific gadids. Polar Biology 39, 1127-1135.

Laurel, B.J., Copeman, L.A., Spencer, M., Iseri, P., 2017. Temperature-dependent growth as a function of size and age in juvenile Arctic cod (*Boreogadus saida*). ICES Journal of Marine Science 74, 1614-1621.

Laurel, B.J., Copeman, L.A., Spencer, M., Iseri, P., 2018. Comparative effects of temperature on rates of development and survival of eggs and yolk-sac larvae of Arctic cod (*Boreogadus saida*) and walleye pollock (*Gadus chalcogrammus*). ICES Journal of Marine Science 75 (7), 2403-2412.

Leis, J.M., 2007. Behaviour as input for modelling dispersal of fish larvae: behaviour, biogeography, hydrodynamics, ontogeny, physiology and phylogeny meet hydrography. Marine Ecology Progress Series 347, 185-193.

Leis, J.M., Carson-Ewart, B.M., 1997. In situ swimming speeds of the late pelagic larvae of some Indo-Pacific coral-reef fishes. Marine Ecology Progress Series 159, 165-174.

Leis, J.M., Carson-Ewart, B.M., 1999. In situ swimming and settlement behaviour of larvae of an Indo-Pacific coral-reef fish, the coral trout *Plectropomus leopardus* (Pisces: Serranidae). Marine Biology 134 (1), 51-64.

Levine, R. M., De Robertis, A., Grünbaum, D., Woodgate, R., Mordy, C. W., Mueter, F., Cokelet, E., Lawrence-Slavas, N., Tabisola, H. 2020. Autonomous vehicle surveys indicate that flow reversals retain juvenile fishes in a highly advective high-latitude ecosystem. Limnology and Oceanography. doi: 10.1002/lno.11671.

Litvak, M.K., Leggett, W.C., 1992. Age and size-selective predation on larval fishes: the bigger-is-better hypothesis revisited. Marine Ecology Progress Series 81, 13-24.

Logerwell, E., Busby, M., Carothers, C., Cotton, S., Duffy-Anderson, J., Farley, E., Goddard, P., Heintz, R., Holladay, B., Horne, J., Johnson, S., 2015. Fish communities across a spectrum of habitats in the western Beaufort Sea and Chukchi Sea. Progress in Oceanography 136, 115-132.

Lovvorn, J.R., Rocha, A.R., Danielson, S.L., Cooper, L.W., Grebmeier, J.M., Hedstrom, K.S., 2020. Predicting sediment organic carbon and related food web types from a physical oceanographic model on a subarctic shelf. Marine Ecology Progress Series 633, 37-54.

Lu, K., Danielson, S., Hedstrom, K., Weingartner, T., 2020a. Assessing the role of oceanic heat fluxes on ice ablation of the central Chukchi Sea Shelf. Progress in Oceanography.

Lu, K., Danielson, S., Weingartner, T., 2020b. Impacts of short-term wind events on Chukchi hydrography and sea ice retreat, Deep Sea Research II.

Luchin, V., Panteleev, G., 2014. Thermal regimes in the Chukchi Sea from 1941 to 2008. Deep Sea Research Part II: Topical Studies in Oceanography 109, 14-26.

Marsh, J.M., Mueter, F.J., Quinn II, T.J., 2019. Environmental and biological influences on the distribution and population dynamics of polar cod (*Boreogadus saida*) in the US Chukchi Sea. Polar Biology. doi: 10.1007/s00300-019-02561-w

Matarese, A.C., Kendall, A.W., Blood, D.M., Vinter, B.M., 1989. Laboratory guide to early life history stages of northeast Pacific fishes. U.S. National Archives and Records Administration, College Park.

Mecklenburg, C.W., Mecklenburg, T.A., Thorsteinson, L.K., 2002. Fishes of Alaska, American Fisheries Society, Bethesda, MD.

Meredith, M., Sommerkorn, M., Cassotta, S., Derksen, C., Ekaykin, A., Hollowed, A., Kofinas, G., Mackintosh, A., Melbourne-Thomas, J., Muelbert, M.M.C., Ottersen, G., Pritchard, H., Schuur, E.A.G., 2019. Chapter 3:Polar Regions. In: IPCC Special Report on the Ocean and Cryosphere in a Changing Climate. Pörtner, H-O., Roberts, D.C., Masson-Delmotte, V.,Zhai, P., Tignor, M., Poloczanska, E., Mintenbeck, K., Alegría, A., Nicolai, M., Okem, A., Petzold, J., Rama, B., Weyer, N.M. (Eds.). https://www.ipcc.ch/site/assets/uploads/sites/3/2019/11/07_SROCC_Ch03_FINAL.pdf

Miller, T.J., 2007. Contribution of individual-based coupled physical–biological models to understanding recruitment in marine fish populations. Marine Ecology Progress Series 347, 127-138.

Moore, S.E., Stabeno, P.J., 2015. Synthesis of Arctic Research (SOAR) in marine ecosystems of

the Pacific Arctic. Progress in Oceanography 136, 1-11.

Morrow, J.E., 1980. The freshwater fishes of Alaska. Alaska Northwest Publishing Company, Anchorage.

Mueter, F.J., Ladd, C., Palmer, M.C., Norcross, B.L., 2006. Bottom-up and top-down controls of walleye pollock (*Theragra chalcogramma*) on the Eastern Bering Sea shelf. Progress in Oceanography 68 (2), 152-183.

Mueter, F.J., Weems, J., Farley, E.V., Sigler, M.F., 2017. Arctic ecosystem integrated survey (Arctic Eis): marine ecosystem dynamics in the rapidly changing Pacific Arctic Gateway. Deep Sea Research Part II 135, 1-6.

National Oceanic and Atmospheric Administration, 2019. Bering Climate: A Current View of the Bering Sea Ecosystem and Climate. Accessed 6 June, 2019. http://www.beringclimate.noaa.gov/data/index.php

Norcross, B.L., Shaw, R.F., 1984. Oceanic and estuarine transport of fish eggs and larvae: a review. Transactions of the American Fisheries Society 113 (2), 153-165.

Norcross, B.L., Holladay, B.A., Busby, M.A., Mier, K., 2006. RUSALCA–Fisheries Ecology and Oceanography. Final Report CIFAR# NA17RJ1224.

Okkonen, S., Ashjian, C., Campbell, R.G., Alatalo, P., 2019. The encoding of wind forcing into the Pacific-Arctic pressure head, Chukchi Sea ice retreat and late-summer Barrow Canyon water masses. Deep Sea Research Part II 162, 22-31.

Okubo, A., 1971. Oceanic diffusion diagrams. Deep Sea Research and Oceanographic Abstracts 18, 789-802.

Olla, B.L., Davis, M.W., Ryer, C.H., Sogard, S.M., 1996. Behavioural determinants of distribution and survival in early stages of walleye pollock, *Theragra chalcogrammai* a synthesis of experimental studies. Fisheries Oceanography 5, 167-178.

Overland, J.E., Bond, N.A., Adams, J.M., 2002. The relation of surface forcing of the Bering Sea to large-scale climate patterns. Deep-Sea Research Part II 49 (26), 5855-5868.

Panteleev, G., Yaremchuk, M., Francis, O., Kikuchi, T., 2013. Configuring high frequency radar observations in the Southern Chukchi Sea. Polar Science 7 (2), 72-81.

Parada, C., Armstrong, D.A., Ernst, B., Hinckley, S. and Orensanz, J.M., 2010. Spatial dynamics of snow crab (*Chionoecetes opilio*) in the eastern Bering Sea—putting together the pieces of the puzzle. Bulletin of Marine Science 86 (2), 413-437.

Peck, M.A., Buckley, L.J., Bengtson, D.A., 2006. Effects of temperature and body size on the swimming speed of larval and juvenile Atlantic cod (*Gadus morhua*): implications for individual-based modelling. Environmental Biology of Fishes 75 (4), 419-429.

Perrette, M., Yool, A., Quartly, G.D., Popova, E.E., 2011. Near-ubiquity of ice-edge blooms in the Arctic. Biogeosciences 8 (2), 515-524.

Petrik, C.M., Duffy-Anderson, J.T., Mueter, F., Hedstrom, K., Curchitser, E.N., 2015. Biophysical transport model suggests climate variability determines distribution of Walleye Pollock early life stages in the eastern Bering Sea through effects on spawning. Progress in Oceanography 138, 459-474.

Petrik, C.M., Duffy-Anderson, J.T., Castruccio, F., Curchitser, E.N., Danielson, S.L., Hedstrom, K., Mueter, F., 2016. Modelled connectivity between Walleye Pollock (*Gadus chalcogrammus*) spawning and age-0 nursery areas in warm and cold years with implications for juvenile survival. ICES Journal of Marine Science 73, 1890-1900.

Pickart, R.S., 2004. Shelfbreak circulation in the Alaskan Beaufort Sea: Mean structure and variability. Journal of Geophysical Research: Oceans, 109 (C4).

Pickart, R.S., Pratt, L.J., Torres, D.J., Whitledge, T.E., Proshutinsky, A.Y., Aagaard, K., Agnew, T.A., Moore, G.W.K., Dail, H.J., 2010. Evolution and dynamics of the flow through Herald Canyon in the western Chukchi Sea. Deep Sea Research Part II 57 (1-2), 5-26.

Ponomarenko, V.P., 1968. Some data on the distribution and migrations of polar cod in the seas of the Soviet Arctic. Rapports et procès-verbaux des reunions/Conseil Permanent International pour l'Exploration de la Mer 158, 131-135.

Ponomarenko, V.P., 2000. Eggs, larvae, and juveniles of polar cod *Boreogadus saida* in the Barents, Kara, and White Seas. Journal of Ichthyology 40 (2), 165-173.

Porter, S.M., Bailey, K.M., 2007. Optimization of feeding and growth conditions for walleye pollock *Theragra chalcogramma* (Pallas) larvae reared in the laboratory. AFSC Processed Report 2007-06. Alaska Fisheries Science Center, NOAA, National Marine Fisheries Service, 7600 Sand Point Way NE, Seattle WA 98115. 20 pp.

R Core Team, 2018. R: A language and environment for statistical computing. R Foundation for Statistical Computing, Vienna, Austria. http://www.R-project.org/

Rand, K., Logerwell, E., Bluhm, B., Chenelot, H., Danielson, S., Iken, K., Sousa, L., 2018. Using biological traits and environmental variables to characterize two Arctic epibenthic invertebrate communities in and adjacent to Barrow Canyon. Deep Sea Research Part II 152, 154-169.

Rienecker, M.M., Suarez, M.J., Gelaro, R., Todling, R., Bacmeister, J., Liu, E., Bosilovich, M.G., Schubert, S.D., Takacs, L., Kim, G.K., Bloom, S., 2011. MERRA: NASA's modern-era retrospective analysis for research and applications. Journal of Climate 24 (14), 3624-3648.

Sambrotto, R.N., Goering, J.J., McRoy, C.P., 1984. Large yearly production of phytoplankton in the western Bering Strait. Science 225, 1147-1150.

Sargent, J., McEvoy, L., Estevez, A., Bell, G., Bell, M., Henderson, J., Tocher, D., 1999. Lipid nutrition of marine fish during early development: current status and future directions. Aquaculture 179 (1-4), 217-229.

Screen, J.A., Simmonds, I., 2010. The central role of diminishing sea ice in recent Arctic temperature amplification. Nature 464 (7293), 1334-1337.

Shchepetkin, A.F., McWilliams, J.C., 2005. The regional oceanic modeling system (ROMS): a split-explicit, free-surface, topography-following-coordinate oceanic model. Ocean Modelling 9, 347-404.

Skopeliti, A., Tsoulos, L., 2013. Choosing a suitable projection for navigation in the arctic. Marine Geodesy 36 (2), 234-259.

Søreide, J.E., Leu, E., Berge, J., Graeve, M., Falk-Petersen, S., 2010) Timing of blooms, algal food quality and *Calanus glacialis* reproduction and growth in a changing Arctic. Global change biology 16 (11), 3154-3163.

Spencer, M.H., Vestfals, C.D., Mueter, F.J., Laurel, B.J., 2020. Ontogenetic changes in the buoyancy and salinity tolerance of eggs and larvae of polar cod (*Boreogadus saida*) and other gadids. Polar Biology. https://doi.org/10.1007/s00300-020-02620-7.

Stabeno, P., Kachel, N., Ladd, C., Woodgate, R., 2018. Flow patterns in the eastern Chukchi Sea: 2010–2015. Journal of Geophysical Research: Oceans 123 (2), 1177-1195.

Stammerjohn, S., Massom, R., Rind, D., Martinson, D., 2012. Regions of rapid sea ice change: an inter-hemispheric seasonal comparison. Geophysical Research Letters 39, L05502.

Stigebrandt, A., 1984. The North Pacific: a global-scale estuary. Journal of Physical Oceanography 14, 464-470.

Sundby, S., Fossum, P. 1990. Feeding conditions of Arcto-Norwegian cod larvae compared with the Rothschild–Osborn theory on small-scale turbulence and plankton contact rates. Journal of Plankton Research 12 (6), 1153-1162.

Sunnanå, K., Christiansen, J.S., 1997. Kommersielt fiske på polar torskerfaringer og potensiale. Fiskeriforsknings Rapportserie 1:20. (In Norwegian).

Thanassekos, S., Fortier, L., 2012. An individual based model of Arctic cod (*Boreogadus saida*) early life in Arctic polynyas: I. Simulated growth in relation to hatch date in the Northeast Water (Greenland Sea) and the North Water (Baffin Bay). Journal of Marine Systems 93, 25-38.

Thompson, D.W.J., Wallace, J.M., 1998. The Arctic Oscillation signature in wintertime geopotential height and temperature fields. Geophysical Research Letters 25, 1297-1300.

Thompson, D.W.J., Wallace, J.M., 2000. Annular modes in the extratropical circulation. Part I: Month-to-month variability. Journal of Climate 13 (5), 1000-1016.

Vestfals, C.D., Ciannelli, L., Duffy-Anderson, J.T., Ladd, C., 2014. Effects of seasonal and interannual variability in along-shelf and cross-shelf transport on groundfish recruitment in the eastern Bering Sea. Deep Sea Research Part II: Topical Studies in Oceanography 109, 190-203.

Vestfals, C.D., Mueter, F.J., Duffy-Anderson, J.T., Busby, M.S., De Robertis, A., 2019. Spatio-temporal distribution of polar cod (*Boreogadus saida*) and saffron cod (*Eleginus gracilis*) early life stages in the Pacific Arctic. Polar Biology 42 (5), 969-990.

Vikebø, F., Jørgensen, C., Kristiansen, T., Fiksen, Ø., 2007. Drift, growth, and survival of larval Northeast Polar cod with simple rules of behaviour. Marine Ecology Progress Series, 347, 207-220.

Vikebø, F., Sundby, S., Ådlandsvik, B., Fiksen, Ø., 2005. The combined effect of transport and temperature on distribution and growth of larvae and pelagic juveniles of Arcto-Norwegian cod. ICES Journal of Marine Science 62 (7), 1375-1386.

Wassmann, P., Duarte, C.M., Agusti, S., Sejr, M.K., 2011. Footprints of climate change in the Arctic marine ecosystem. Global change biology 17 (2), 1235-1249.

Watanabe, E., Wang, J., Sumi, A. and Hasumi, H., 2006. Arctic dipole anomaly and its contribution to sea ice export from the Arctic Ocean in the 20th century. Geophysical Research Letters, 33 (23).

Weingartner, T., Aagaard, K., Woodgate, R., Danielson, S., Sasaki, Y., Cavalieri, D., 2005. Circulation on the north central Chukchi Sea shelf. Deep Sea Research Part II 52, 3150-3174.

Whitefield, J., Winsor, P., McClelland, J., Menemenlis, D., 2015. A new river discharge and river temperature climatology data set for the pan-Arctic region. Ocean Modelling 88: 1-15.

Whitehouse, G.A., 2011. Modeling the eastern Chukchi Sea food web with a mass-balance approach. Ph.D. thesis, University of Washington, unpublished.

Wilderbuer, T.K., Hollowed, A.B., Ingraham, W.J., 2002. Flatfish recruitment response to decadal climatic variability and ocean conditions in the eastern Bering Sea. Progress in Oceanography 55 (1-2), 235-247.

Winsor, P., Chapman, D.C., 2004. Pathways of Pacific water across the Chukchi Sea: A numerical model study. Journal of Geophysical Research: Oceans, 109 (C3).

Woillez, M., Rivoirard, J., Petitgas, P., 2009. Notes on survey-based spatial indicators for monitoring fish populations. Aquatic Living Resources 22 (2), 155-164.

Wolotira, R.J. Jr, 1985. Saffron cod (*Eleginus gracilis*) in western Alaska: the resource and its potential. Northwest and Alaska Fisheries Center, Kodiak.

Woodbury, D., Hollowed, A.B., Pearce, J.A., 1995. Interannual variation in growth rates and back-calculated spawn dates of juvenile Pacific hake (*Merluccius productus*). In: Recent Developments in Fish Otolith Research. Secor, D.H., Dean, J.M., Campana, S.E. (Eds.), Belle W. Baruch Institute for Marine Biology and Coastal Research, University of South Carolina Press, Columbia, SC, pp. 481-496.

Woodgate, R.A., 2018. Increases in the Pacific inflow to the Arctic from 1990 to 2015, and insights into seasonal trends and driving mechanisms from year-round Bering Strait mooring data. Progress in Oceanography 160, 124-154.

Woodgate, R.A., Stafford, K.M., Prahl, F.G., 2015. A synthesis of year-round interdisciplinary mooring measurements in the Bering Strait (1990–2014) and the RUSALCA years (2004–2011). Oceanography 28 (3), 46-67.

Woodgate, R.A., Aagaard, K., 2005. Revising the Bering Strait freshwater flux into the Arctic Ocean. Geophysical Research Letters 32 (2). https://doi.org/10.1029/2004GL021747.

Woodgate, R.A., Aagaard, K., Weingartner, T.J., 2005a. Monthly temperature, salinity, and transport variability of the Bering Strait through flow. Geophysical Research Letters 32, L04601. https://doi.org/10.1029/2004GL021880.

Woodgate, R.A., Aagaard, K., Weingartner, T.J., 2005b. A year in the physical oceanography of the Chukchi Sea: moored measurements from autumn 1990–1991. Deep-Sea Research Part II 52 (24-26), 3116-3149.

Wu, B., Wang, J., Walsh, J.E., 2006. Dipole anomaly in the winter Arctic atmosphere and its association with sea ice motion. Journal of Climate 19(2), 210-225.

Wyllie-Echeverria, T., Barber, W.E., Wyllie-Echeverria, S., 1997. Water masses and transport of age-0 Arctic Cod and age-0 Bering flounder into the northeastern Chukchi Sea. In: Fish ecology in Arctic North America. Reynolds, J.B. (Ed.), American Fisheries Society Symposium 19. American Fisheries Society, Bethesda, MD, pp. 60-67.

Yudanov, I.G., 1976. Zoogeography of polar cod in the Arctic Ocean. Priroda i Khoziaistvo Severa (Nature and Economy of the North), vol 4. KNTs RAN, Apatity, 111-113.